A census of the Wolf-Rayet content in Westerlund 1 from near-infrared imaging and spectroscopy

Journal Item

Mon. Not. R. Astron. Soc. **000**, 1–?? (2006) Printed 5 February 2008 (MN LATEX style file v2.2)

A census of the Wolf-Rayet content in Westerlund 1 from near-infrared imaging and spectroscopy⋆

Paul A. Crowther[1], L. J. Hadfield[1], J. S. Clark[2], I. Negueruela[3] and W. D. Vacca[4]
[1] *Department of Physics & Astronomy, University of Sheffield, Hicks Building, Hounsfield Rd, Sheffield, S3 7RH, UK*
[2] *Department of Physics & Astronomy, The Open University, Milton Keynes, MK7 6AA, UK*
[3] *Dpto de Fisica, Ingenieria de Sistemas y Teoria de la Senal, Universidad de Alicante, Apdo. 99, E03080, Alicante, Spain*
[4] *SOFIA-URSA, NASA Ames Research Center, MS N211-3, Moffett Field, CA 94035, USA*

Accepted 2006 Aug 16; Received 2006 August 2; in original form 2006 Jul 21

ABSTRACT
New NTT/SOFI imaging and spectroscopy of the Wolf-Rayet population in Westerlund 1 are presented. Narrow-band near-IR imaging together with follow up spectroscopy reveals four new Wolf-Rayet stars, of which three were independently identified recently by Groh et al., bringing the confirmed Wolf-Rayet content to 24 (23 excluding source S) – representing 8% of the known Galactic Wolf-Rayet population – comprising 8 WC stars and 16 (15) WN stars. Revised coordinates and near-IR photometry are presented, whilst a quantitative near-IR spectral classification scheme for Wolf-Rayet stars is presented and applied to members of Westerlund 1. Late subtypes are dominant, with no subtypes earlier than WN5 or WC8 for the nitrogen and carbon sequences, respectively. A qualitative inspection of the WN stars suggests that most (∼75%) are highly H-deficient. The Wolf-Rayet binary fraction is high (⩾62%), on the basis of dust emission from WC stars, in addition to a significant WN binary fraction from hard X-ray detections according to Clark et al. We exploit the large WN population of Westerlund 1 to reassess its distance (∼5.0 kpc) and extinction ($A_{K_S} \sim 0.96$ mag), such that it is located at the edge of the Galactic bar, with an oxygen metallicity ∼60% higher than Orion. The observed ratio of WR stars to red and yellow hypergiants, N(WR)/N(RSG+YHG) ∼ 3, favours an age of ∼4.5–5.0 Myr, with individual Wolf-Rayet stars descended from progenitors of initial mass $\sim 40 - 55 M_{\odot}$. Qualitative estimates of current masses for non-dusty, H-free WR stars are presented, revealing $10 - 18 M_{\odot}$, such that ∼75% of the initial stellar mass has been removed via stellar winds or close binary evolution. We present a revision to the cluster turn-off mass for other Milky Way clusters in which Wolf-Rayet stars are known, based upon the latest temperature calibration for OB stars. Finally, comparisons between the observed WR population and subtype distribution in Westerlund 1 and instantaneous burst evolutionary synthesis models are presented.

Key words: stars: Wolf-Rayet – open clusters: individual (Westerlund 1)

1 INTRODUCTION

Several hundred Wolf-Rayet (WR) stars – the evolved descendants of the most massive O stars – have been identified within the Milky Way (van der Hucht 2006). In principle, studies of WR stars in open clusters provides excellent observational constraints upon their ages and initial masses (e.g. Schild & Maeder 1984). In practice, this has proved challenging, due to the small number of WR stars observed within individual Milky Way or Magellanic Cloud clusters. This is unsurprising, given their short lifetimes and small number of suitably massive stars in typical open clusters ($\approx 10^3 M_{\odot}$), for which empirical studies indicate a maximum stellar mass of $\sim 30 - 35 M_{\odot}$ (e.g. Weidner & Kroupa 2006). Hitherto, solely the Arches, Quintuplet and Galactic Centre clusters have offered the potential for studying large numbers of WR stars in suitably massive ($10^4 M_{\odot}$) clusters, for which significantly higher mass stars are observed, albeit hindered by exceptionally high interstellar extinction.

Fortunately, Westerlund 1 (Westerlund 1961) offers the possibility of undertaking a comprehensive study of WR stars at Solar or moderately super-Solar metallicity, since its mass has been estimated at $10^5 M_{\odot}$ (Clark et al. 2005). Instantaneous burst evolutionary synthesis models at Solar metallicity (e.g. Starburst99, Leitherer et al. 1999) predict 20–30 WR stars at an age of 4.5 Myr for such a high cluster mass. Observationally, Clark & Negueruela (2002), Negueruela & Clark (2005) and Hopewell et al. (2005) have identified 20 WR stars within 4 arcmin (∼6 pc at a distance

⋆ Based on observations made with ESO telescopes at the La Silla Observatory under programme IDs 073.D-0321 and 075.D-0469

Table 1. Catalogue of Wolf-Rayet stars in Westerlund 1, including WR nomenclature following van der Hucht (2006), following previous studies by Clark & Negueruela (2002, CN02), Negueruela & Clark (2005, NC05), Hopewell et al. (2005, H05), Negueruela (2005, priv comm, N05) and Groh et al. (2006, G06). Photometry is obtained primarily from NTT/SOFI or 2MASS (Skrutskie et al. 2006). Coordinates are obtained from our NTT/SOFI images, except where noted, based upon astrometry of A–G from 3.6cm radio images (see CN02). Previously published coordinates for I and J were in error due to spatial crowding.

Source	Alias	WR	α	δ	J	H	K_S	Ref	Previous	Ref	This
			J2000		mag	mag	mag		Sp Type		Study
A	Wd1-72	WR77sc	16 47 08.32	–45 50 45.5	10.34	9.11:	8.37:	SOFI	WN4–5, <WN7	CN02, NC05	WN7b
B		WR77o	16 47 05.36	–45 51 05.0	10.91	9.79	9.18	SOFI	WNL, WN8?	CN02, NC05	WN7o
C		WR77m	16 47 04.40	–45 51 03.8	11.26	9.51	8.23	SOFI	WC8, WC8.5	CN02, NC05	WC9d
D		WR77r	16 47 06.24	–45 51 26.5	11.63	10.31	9.61	SOFI	WN6–8	CN02	WN7o
E	Wd1-241	WR77p	16 47 06.05	–45 52 08.2	10.12	9.09	8.29:	SOFI	WC9	CN02	WC9
F	Wd1-239	WR77n	16 47 05.22	–45 52 25.0	9.85	7.97	7.28	SOFI	WC9	CN02	WC9d
G		WR77j	16 47 04.01	–45 51 25.2	11.36	9.97	9.28	SOFI	WN6–8	CN02	WN7o
H		WR77l	16 47 04.22	–45 51 20.2	10.31	8.56	7.38	SOFI	WC9	CN02	WC9d
I		WR77c	16 47 00.88	–45 51 20.8	10.89	9.57	8.86	SOFI	WN6–8	CN02	WN8o
J		WR77e	16 47 02.47	–45 51 00.1	11.7:	10.3:	9.7:	SOFI	WNL	CN02	WN5h
K		WR77g	16 47 03.25	–45 50 43.8	11.81	10.40	9.53	SOFI	WC, WC7	CN02, NC05	WC8
L	Wd1-44	WR77k	16 47 04.19	–45 51 07.4	9.08	7.72	7.19	SOFI	WN9	NC05	WN9h:
M	Wd1-66	WR77i	16 47 03.96	–45 51 37.8	10.13	7.64	6.9:	SOFI	WC9	NC05	WC9d
N		WR77b	16 46 59.9	–45 55 26	9.69	7.84	6.41	2MASS	WC8	NC05	WC9d
O		WR77sb	16 47 07.66	–45 52 35.9	11.00	9.98	9.45	SOFI	WN6	NC05	WN6o
P	Wd1-57c	WR77d	16 47 01.59	–45 51 45.5	11.06	9.83	9.26	SOFI	WN8	NC03	WN7o
Q		WR77a	16 46 55.55	–45 51 35.0	11.72	10.67	10.00	SOFI	WN6–7	NC05	WN6o
R	Wd1-14c	WR77q	16 47 06.07	–45 50 22.6	11.92	10.84	10.26	SOFI	WN6–7	NC05	WN5o
S	Wd1-5	WR77f	16 47 02.98	–45 50 20.0	9.81	8.80:	8.29	SOFI	WNVL	NC05	WN10-11h or B0–1Ia$^+$
T	HBD4	WR77aa	16 46 46.3	–45 47 58	10.04	8.21	6.72	2MASS	WC9d	H05	WC9d
U	#1	WR77s	16 47 06.55	–45 50 39.0	10.77	9.72	9.20	SOFI	WN4, WN5–7	N05, G06	WN6o
V		WR77h	16 47 03.81	–45 50 38.8	10.75	9.42	8.76	SOFI	WN8	N05	WN8o
W	#3	WR77sa	16 47 07.58	–45 49 22.2	12.11	10.75	10.04	SOFI	WN5–6	G06	WN6h
X	#2	WR77sd	16 47 14.1	–45 48 32	12.36	11.08	10.25	2MASS	WN4–5	G06	WN5o

of 5 kpc) of the central cluster, most of which were discovered serendipitously.

The present study examines the Wolf-Rayet content of Westerlund 1 based upon near-infrared narrow-band imaging and follow up spectroscopy. High interstellar extinction (A_V= 11.6 mag, Clark et al. 2005) prohibits the standard optical approach of using a narrow-band He II λ4686 filter and adjacent continuum filter to identify WR candidates (e.g. Hadfield et al. 2005). Homeier et al. (2003ab) have previously used interference filters within the K-band to identify WR candidates within the inner Milky Way. However, in contrast to the optical technique, the K-band is observationally more challenging since (i) WR line fluxes are much weaker; (ii) there is no single pair of interference filters that can applied to identify all WR subtypes; (iii) dust emission in WC stars may heavily dilute the WR stellar emission line fluxes.

The present paper is structured as follows. New K-band and Y-band imaging of Westerlund 1 is presented in Sect. 2 together with near-IR spectroscopy. Near-IR spectral classification of WR stars in Westerlund 1 is presented in Sect. 3. The reddening and distance to Westerlund 1 are reassessed from its WR population in Sect. 4, and comparisons made with other Milky Way clusters hosting WR stars. The observed WR content of Westerlund 1 is compared to predictions from single and binary models in Sect 6. Finally, brief conclusions are drawn in Sect. 7

2 NEAR-IR OBSERVATIONS OF WESTERLUND 1

Here we present new near-IR imaging and spectroscopy of Westerlund 1, obtained with the 3.5m New Technology Telescope (NTT), La Silla, Chile, using the "Son of Isaac" (SOFI) instrument.

2.1 Narrow-band Imaging

A series of NTT/SOFI narrow-band images were obtained for the central (4.9 $\times$4.9 arcmin) region of Westerlund 1 on 1 May 2004 (ESO programme 073.D-0321(C)) using the standard plate scale of 0.288 arcsec/pix and Hawaii HgCdTe 1024 $\times$ 1024 array. The interference filters used were the 2.07μm (He I), 2.09μm (C IV), 2.13μm (continuum), 2.17μm (Brγ), 2.19μm (He II) and 2.25μm (continuum), each with FWHM = 0.02 – 0.03μm. The jittered images for Wd 1 and Hipparcos standard stars were reduced using ORAC-DR (Economou et al. 2004). Our Brγ-band image of the central cluster (FWHM $\sim$ 0.7 arcsec) is presented in the lower panel of Fig. 1, together with WR stars indicated, plus W9 (sgB[e]) and W243 (LBV, Clark et al. 2005). Four WR stars lie beyond the central region, which are indicated in the 10$\times$10 arcmin *Spitzer* IRAC (3.6μm) image shown in the upper panel of Fig. 1, taken from the GLIMPSE survey (Benjamin et al. 2003).

Images were prepared following standard procedures, with photometry obtained using DAOPHOT within IRAF, with typical uncertainties of $\pm$0.1 mag.

In principle, different pairs of filters should permit the identification of different WN and WC subtypes. Late type WN and WC subtypes, with strong He I 2.058μm emission (Crowther & Smith 1996; Eenens et al. 1991), are anticipated to be brighter in the 2.07μm filter than at 2.09μm. Early and mid-WN stars, with strong He II 2.189μm emission (Crowther & Smith 1996) should be brighter in the 2.19μm filter than at 2.25μm. Finally, early and mid-WC stars should be much brighter in the 2.07μm filter than at 2.12μm due to very strong C IV 2.08μm emission (Eenens et al. 1991). Complications will arise in case of dust emission, leading to a dilution of emission line strengths, or extremely high interstellar

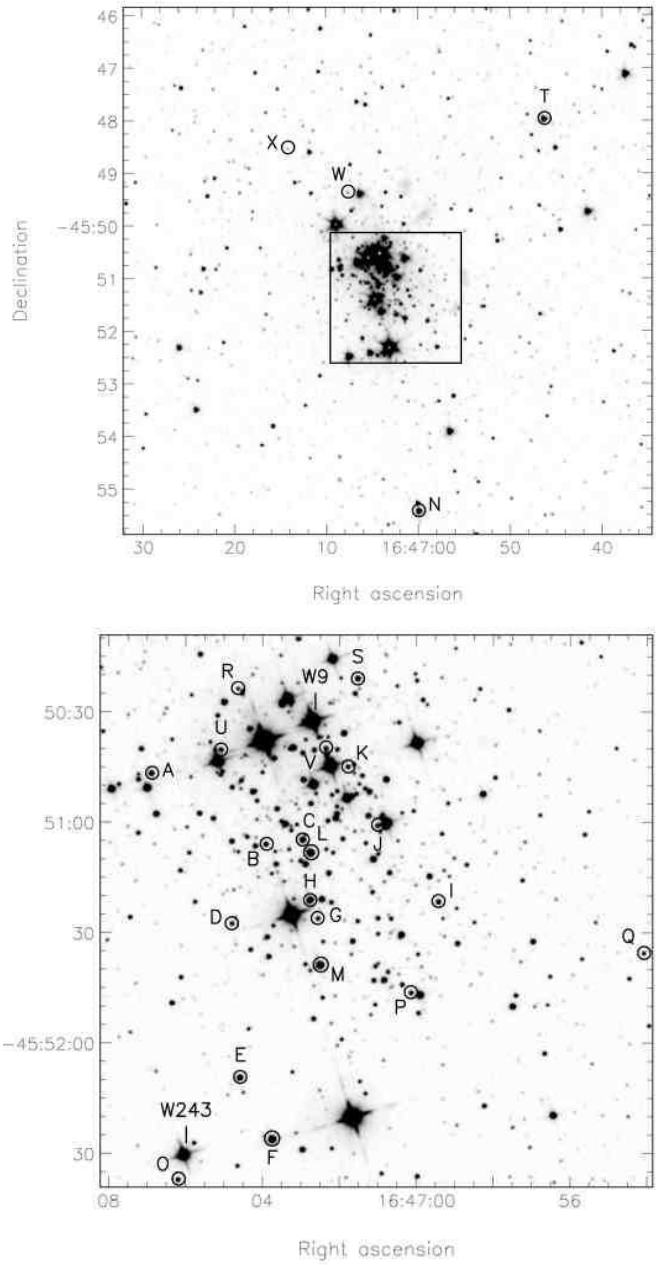

Figure 1. (upper panel) *Spitzer* IRAC (3.6μm) image of the 10×10 arcmin (15 ×15 pc at a distance of 5 kpc) region surrounding Westerlund 1 surveyed with NTT/SOFI, taken from the GLIMPSE survey (Benjamin et al. 2003). Identifications of the four WR stars located beyond the cluster centre (shown as a box); (lower panel) ESO/NTT SOFI Brγ image of the central 2.5×2.5 arcmin (3.75×3.75 pc) of Westerlund 1, for which the Wolf-Rayet stars have been indicated, plus W9 (sgB[e]) and W243 (LBV, Clark et al. 2005). North is up, with east to the left in both images.

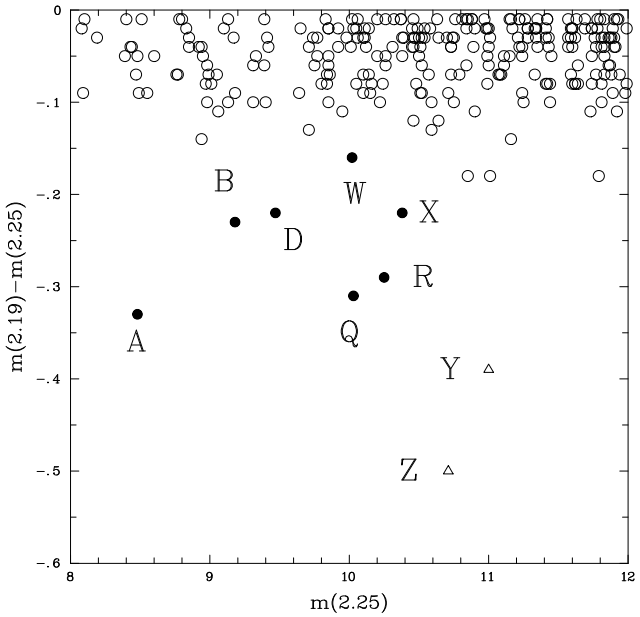

Figure 2. Comparison between SOFI interference filter photometry of the central cluster at 2.189μm (He II) and 2.25μm (continuum). The 2.25μm zero point has been defined using K_S-band magnitudes for our WR stars. Strong He II emission is observed for known early-type WN stars within Westerlund 1 (filled circles), including our newly identified candidates W and X, Y and Z, for which the latter two were not spectroscopically confirmed (open triangles, see text).

extinction, leading to differences between the continua across the K-band.

From our anticipated combinations, the most useful proved to be the [2.19] – [2.25] pair, for which several known mid-type WN stars exhibited large ∼0.3 mag excesses in the 2.19μm filter. Four additional candidates revealed an excess of at least 0.15 mag, which we have labelled as W, X, Y, Z, following our previous nomenclature for WR stars in Westerlund 1, which ended at S (Negueruela & Clark 2005), supplemented by WR77aa from Hopewell et al. (2005), which we shall denote as source T hereafter plus U and V previously discovered from optical spectroscopy by Negueruela (2005, priv. comm.).

The [2.19] – [2.25] colour magnitude diagram is presented in Figure 2. We set the zero point of the 2.25μm filter to the K_S-band magnitude for simplicity since no flux standards were taken with this filter set. The Figure illustrates how the known WN stars in Westerlund 1, A, B, D, Q and R, display the expected He II 2.189μm excess. Following the completion of our study, Groh et al. (2006) presented their own Y-band imaging of Westerlund 1 which highlighted sources W (their #3) and X (their #2), plus follow-up spectroscopy that included source U (their #1).

The other combinations revealed only one suitable match between them, i.e. star E (WC9) which showed an excess in the [2.07] – [2.09] diagram. Other late WN or WC stars previously known in Westerlund 1 were not identified from these images, although some of the brighter stars were saturated. Our spectroscopy (Sect 3) revealed that line dilution by dust emission was responsible for the lack of [2.07] – [2.09] excess in several WR stars. Finally, no evidence for early WC stars was found from a comparison between the 2.07μm and 2.12μm images. Either early type WC stars are absent in Westerlund 1 or dust dilution would need to be very severe to prevent their identification from narrow-band imaging. For example, K-band emission lines are seen during dust formation in the case of WR140 (WC7+O4–5,Williams 2002).

Two WR stars associated with Westerlund 1 are known to lie at a distance of several arcmin from the cluster core (Fig. 1). Consequently, on 29 Jun 2005, the same SOFI K-band interference filters described above were used to image fields centred ∼4 arcmin to

Table 2. *Spitzer* IRAC point source catalogue photometry from the GLIMPSE survey (Benjamin et al. 2003) and mid-IR colours of selected Wolf-Rayet stars in Westerlund 1, plus red sources within our observed fields exhibiting [1.08] – [1.06] excesses of 0.4 mag or greater (their 2MASS designations are indicated, Skrutskie et al. 2006).

Source	Sp Type	[1.08] – [1.06]	J	J–H	H–K_S	Ref	[3.6]	[4.5]	[5.8]	[8.0]	[3.6]–[4.5]	[5.8]–[8.0]	K_S–[8.0]
D	WN7o	–1.0	11.63	1.32	0.70	SOFI	8.47	8.17	–		0.30	–	–
E	WC9	–1.0	10.12	1.03	0.80	SOFI	7.13	6.71	–	6.14	0.42	–	2.15
I	WN8o	–1.4	10.89	1.32	0.71	SOFI	–	–	7.32	6.96	–	0.36	1.90
N	WC9d		9.69	1.85	1.43	2MASS	–	–	4.32	4.17	–	0.15	2.24
T	WC9d	–1.1:	10.04	1.83	1.49	2MASS	–	–	4.04	4.05	–	0.01	2.67
W	WN6h	–0.8	12.11	1.36	0.71	SOFI	9.01	8.61	8.37	8.01	0.40	0.36	2.03
X	WN5o	–0.5	12.36	1.28	0.83	2MASS	9.32	–	8.71	8.35	–	0.36	1.90
16471179-4548361		–0.4	11.00	2.62	1.27	2MASS	–	–	6.10	6.05	–	0.05	1.05
16464503-4548311		–1.5	11.26	2.53	1.34	2MASS	–	–	5.85	5.52	–	0.33	1.87
16464447-4550044		–0.6	11.42	2.76	1.57	2MASS	–	–	5.77	5.47	–	0.30	1.62

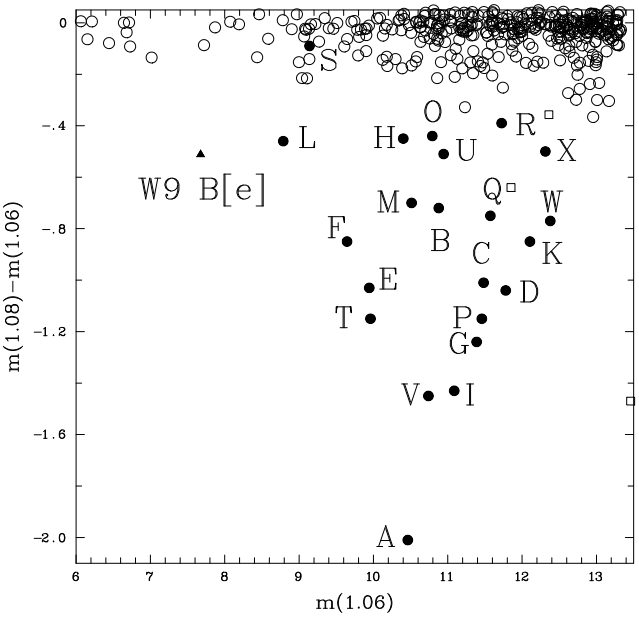

Figure 3. Comparison between SOFI interference filter photometry of the central cluster at 1.08μm (He I) and 1.06μm (continuum), illustrating strong emission for known WN and WC stars (filled circles) plus the B[e] supergiant W9 (filled triangle). The 1.06μm zero point has been defined using J-band magnitudes for a subset of our WR stars, permitting the inclusion of source T and three extremely red sources (open squares) from narrow-band imaging in the NW and NE fields.

the NE, NW, SW and SE, i.e. sampling the 10×10 arcmin region shown in the upper panel of Fig. 1.

In addition, due to the potential diluting influence of a strong dust continuum to the emission lines within the K-band, we obtained images for all pointings using two further Y-band interference filters on 30 Jun 2005, namely 1.06μm (continuum) and 1.08μm (He I). The [1.08] – [1.06] index suffers from a higher sensitivity to extinction with respect to the K-band indices, yet one expects He I 1.083μm to be exceptionally strong in late-type WR stars of both sequences, be present in early-type WR stars, and not suffer the same degree of dust continuum dilution as those obtained in the K-band (e.g. Howarth & Schmutz 1992).

We present the corresponding [1.08] – [1.06] diagram for the entire Westerlund 1 region in Fig. 3. We set the zero point of the 1.06μm filter to the J-band magnitude for simplicity since no flux standards were taken with this filter set. We estimate typical uncertainties of $\pm$0.1 mag, from comparison between photometry of individual sources observed in multiple fields. Fig 3 illustrates the much cleaner identification of WR stars in Westerlund 1, with the exception of source S which possesses unusually weak, narrow He I emission. The extreme B[e] supergiant W9 (Clark et al. 2005) is also a strong He I 1.083μm emitter. All known and candidate WR stars are indicated here except for N which lies at the edge of the SE field, and J which has a very bright close neighbour preventing reliable photometry. A similar comparison has recently been made by Groh et al. (2006) for the central cluster, who also exploited filters centred upon He II 1.01μm and the adjacent continuum. Of course, extremely red sources will also exhibit a large [1.08] – [1.06] excess. Those with excesses greater than 0.4 mag are indicated in the figure, and will be considered in the next section.

2.2 Broad band near-IR imaging and photometry

In addition to our interference band imaging, we obtained jittered J, H and K_S band images of the central region of Westerlund 1 on 24 Sep 2004. These were reduced using ORAC-DR, from which DAOPHOT photometry was obtained, with typical uncertainties of $\pm$0.05 mag. These were supplemented by 2MASS (Skrutskie et al. 2006) J, H, K_S[1] photometry for WR stars which were located beyond the cluster core, where spatial crowding was not so significant. In a few cases SOFI and 2MASS photometry are available - notably for source I, agreement is within 0.01 mag, except that 2MASS indicates a H-band magnitude fainter by 0.09 mag.

A colour-colour diagram for the known WR stars in Westerlund 1 is presented in Figure 4. The scatter amongst WN stars is due to intrinsic colour and extinction variations, whilst the WC stars are offset to higher values, as a result of hot, circumstellar, dust emission, with the exceptions of sources E (WC9) and K (WC8). We shall therefore follow the recent convention in adding 'd' to WC classifications to signify dust emission (e.g. van der Hucht 2006). We shall address the presence or absence of dust in Sect. 5. We also include the three sources displaying a large [1.08] - [1.06] excess in Fig 4, which overlap with the position of the dust forming WC stars.

[1] Note that both NTT/SOFI and 2MASS employ K_S filters ($\lambda_c \sim 2.16\mu$m, FWHM$\sim 0.27\mu$m), in contrast to K′ ($\lambda_c \sim 2.12\mu$m) or K ($\lambda_c \sim 2.20\mu$m) filters, which are commonly used elsewhere.

Table 3. NTT/SOFI emission equivalent widths (in Å, accurate to ±10%) for prominent near-IR lines (wavelengths are in μm) in WN stars in Westerlund 1.

Star	Sp Type	He II 1.012	He I 1.083	He II+Pγ 1.093	He II 1.163	He II+Pβ 1.281	He II 1.476	He II 1.692	He I 1.700	He I 2.058	N V 2.110	He I/N III 2.115	He II+Brγ 2.165	He II 2.189	1.012 /1.083	2.189 /2.165
A	WN7b	280	— 930 —		194	110	113	— 141 —		35	— 74 —		87	123	0.3	1.4
B	WN7o	65	147	12	50	30	28	16:	21:	∼5	3	25	34	36	0.4	1.1
D	WN7o	98	316	21	88	47	39	18	34	13	1	35	68	47	0.3	0.7
G	WN7o	148	443	29	87	58	41	11	34	8	3	34	53	33	0.3	0.6
I	WN8o	54	459	32	44	61	22	7	48	26	3	50	64	17	0.12	0.26
J	WN5h	56	31	8	38	15	22	15	<4	<4	3	12	31	46	1.8	1.5
L	WN9h:	3	72	9	<1	22	<1	<1	11	50	0	7	23	<2	0.04	<0.08
O	WN6o	93	82	7	66	21	37	18	8	4	3	17	20	44	1.1	2.2
P	WN7o	78	285	22	75	41	35	9	23	10	4	34	38	27	0.3	0.7
Q	WN6o	171	159	19	128	43	68	29	12	6	6	27	31	71	1.1	2.3
R	WN5o	168	82	12	109	35	63	31	7	3	8	23	32	94	2.0	2.9
S	WN10-11h: or B0–1Ia$^+$	<2	14	1	<1	8	<1	<1	1	10	0	1	8	<0.5	<0.07	< 0.06
U	WN6o	56	72	6	42	14	27	14	7	4	2	15	17	34	0.8	2.0
V	WN8o	41	326	17	31	43	21	5	39	22	2	37	48	17	0.13	0.35
W	WN6h	113	137	31	86	65	44	20	8	<4	4	19	55	51	0.8	0.9
X	WN5o	214	112	20	134	48	61	31	8	3	9	20	34	98	1.9	2.9

Table 4. NTT/SOFI emission equivalent widths (in Å, accurate to ±10%) for prominent near-IR lines (wavelenths are in μm) in WC stars in Westerlund 1.

Star	Sp Type	C III 0.971	C II 0.990	He II 1.012	He I 1.083	C IV 1.191	C III 1.198	He I/C II 1.700	C IV 1.74	C II 1.785	He I 2.058	C IV 2.076	C III 2.110	He II/C III 2.165	He II 2.189	0.971 /0.990	2.076 /2.110
C	WC9d	305	44	17	191	23	87	15	13	44	44	22	38	11	11	7	0.58
E	WC9	132	31	8	226	10	61	32	12:	65:	153	30	54	30	16	4.3	0.55
F	WC9d	163	22	8	189	8	37	5	2	24	2	<1	3	<1	<1	7.5	<0.3
H	WC9d	89	23	3	84	11	40	9	4	30	37	13	23	9	8	3.9	0.56
K	WC8	509	36	35	132	82	67	43	149	95	— 430 —		198	39	59	14	2.2
M	WC9d	269	53	14	154	11	56	3	<2	14	4	2	7	<1	<1	5.1	0.28
N	WC9d	169	20	11	81	13	23	5	6	9	5	9	11	5	4	8.6	0.8
T	WC9d	345	75	15	281	12	75	12	19	20	27	5	13	5	3	4.6	0.4

Further evidence for the presence of dust emission will be revealed via line dilution in K-band spectroscopy in the next section. Table 2 presents IRAC photometry for those WR stars in Westerlund 1 from the GLIMPSE survey (Benjamin et al. 2003) that are sufficiently isolated, together with mid-IR colours. We also include the three sources displaying a large [1.08] - [1.06] excess. In principle, these represent additional strong He I emission line candidates, although they are extremely red sources as seen from the J-H, H-K and IRAC colours, such that we attribute the [1.08] - [1.06] excess to their extremely red nature. It was possible to test this suggestion for several cases in which SOFI spectroscopy was obtained.

As expected, the mid-IR colours for WN stars are relatively uniform with K_S - [8.0] $\sim$ 1.95 mag, or (K_S - [8.0])$_0$ $\sim$ 1.40 mag after correction for interstellar extinction ($A_{8.0} \sim 0.43 A_{K_S}$, Indebetouw et al. 2005). This is typical of WR stars whose near to mid-IR spectrum is dominated by the free-free excess from the stellar wind superimposed upon the underlying Rayleigh-Jeans tail (e.g. Barlow et al. 1981). Non-LTE stellar atmosphere models (e.g. Hillier & Miller 1998) suggest (K_S - [8.0])$_0$ in the range from ∼1.4 mag for strong-lined WN stars such as WR40 and WR6 (Herald et al. 2001; Morris et al. 2004) to ∼0.6 mag for weak-lined WN stars such as WR3 (e.g. Marchenko et al. 2004). The presence of hot dust in WC stars produces flatter mid-IR colours (e.g. Williams et al. 1987, van der Hucht et al. 1996, Hopewell et al. 2005), as shown in Table 2 (e.g. compare the [5.8] - [8.0] colours for T and N with respect to I, W and X.)

2.3 Spectroscopy

Spectroscopy of known and candidate Wolf-Rayet stars in Westerlund 1 was obtained on 29–30 Jun 2005 with SOFI, using the IJ and HK grisms (programme 075.D-0469). A slit width of 0.6 arcsec provided a resolving power of $R \sim 1000$. In general, position angles were selected in order to simultaneously observe two (or more) targets. Spectroscopic datasets were reduced using IRAF, with wavelength calibration achieved using internal arc lamps. Frequent late B-type Hipparcos standard were obtained at an airmass close to that of Westerlund 1 in order to achieve flux and telluric correction. Photometry from J,H, K_S imaging provided an absolute flux calibration.

The two candidates common to Figs. 2-3, namely W and X were confirmed as Wolf-Rayet stars (see also Groh et al. 2006), whilst sources Y and Z, that appeared to exhibit a strong excess at He II 2.19μm (but not He I 1.08μm) were not. K-band spectroscopy of Y was featureless, whilst source Z displayed 2.3μm CO absorption, typical of late-type giants or supergiants (its J–H colour was also red). The origin of the apparent 2.19μm photometric excess is consequently unclear.

The addition of W and X brings the number of known WR

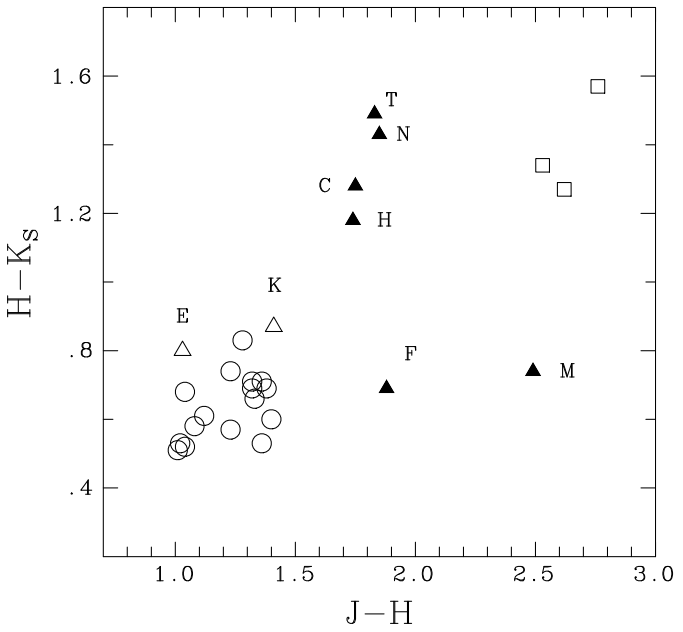

Figure 4. Near-IR colour-colour diagram for Westerlund 1 WN (circles) and WC (triangles) stars, plus three very red sources in the vicinity of Westerlund 1 (squares, Table 2). Dust-forming WC stars are indicated as filled symbols (compare their colours to non-dusty stars E and K).

stars in Westerlund 1 to 24, or 23 if source S is omitted due to its ambiguous nature. Several additional candidates identified from the extended field were observed spectroscopically, including the source with 2MASS designation 16464503-4548311 (Table 2). These sources were not confirmed as WR stars, again revealing CO 2.3μm absorption, such that their [1.08] – [1.06] excess appears to result from intrinsic red colours in such cases.

Spectroscopy of individual WR stars is discussed in the next section, whilst a catalogue of the known WR population in Wd 1 is presented in Table 1. Coordinates were obtained from our SOFI images, except where noted, using astrometry of A–G from 3.6 cm radio images which are nominally accurate to $\pm 0.3''$ (Clark & Negueruela 2002). These differ from previously published coordinates for I and J, as a result of severe crowding within these regions.

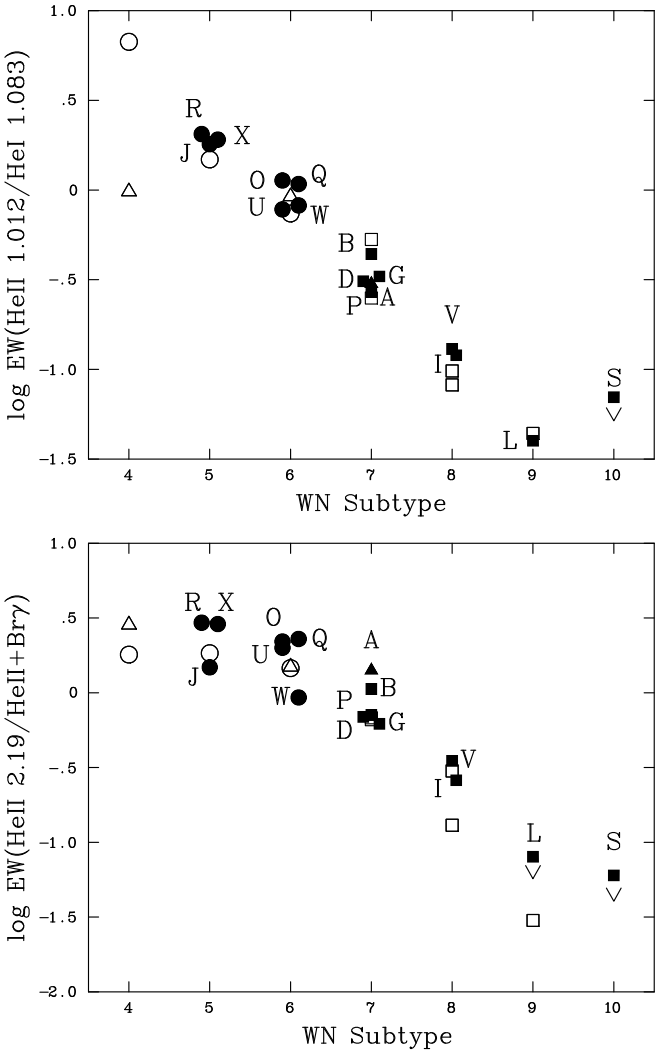

Figure 5. Near-IR diagnostic line ratios for Westerlund 1 WN stars (filled symbols) together with selected optically classified Milky Way stars (WR6, 16, 78, 105, 115, 120, 123, 128, 136, 138, open symbols) for which equivalent width measurements are from Howarth & Schmutz (1992), Crowther & Smith (1996) and Vacca et al. (2006). Weak-lined WNE, strong-lined WNE, and WNL stars are indicated by circles, triangles and squares, respectively.

3 NEAR-IR SPECTRAL CLASSIFICATION OF WR STARS

Several near-IR atlases of WR spectroscopy have previously been presented, notably by Howarth & Schmutz (1992) in the Y-band, and by Crowther & Smith (1996) and Figer et al. (1997) for WN stars and Eenens et al. (1991) for WC stars at longer wavelengths. However, no attempt has previously been made at quantifying subtypes based upon near-IR spectroscopy, with reference to the standard optical criteria of He 5876Å/He II 5411Å for WN subtypes (Smith et al. 1996) and C III 5696Å/C IV 5805Å for WC subtypes (Crowther et al. 1998). In principle, suitable classification diagnostics are available in the near-IR, notably He I 1.083μm/He II 1.012μm for helium and C III 2.110μm/C IV 2.076μm for carbon. Additional line ratios, such as He I 2.058μm/He II 2.189μm and C II 0.990μm/C III 0.971μm are potential secondary diagnostics for late subtypes (these C II and He I lines are very weak in early subtypes). Towards this goal, we have collected line equivalent widths for several WN and WC stars for which optical classifications are well established, based primarily on near-IR spectroscopy from Howarth & Schmutz (1992), Eenens et al. (1991), Crowther & Smith (1996) and Vacca et al. (2006).

Equivalent widths of emission lines in Westerlund 1 have been measured from normalized NTT/SOFI spectroscopy, which are presented for WN and WC subtypes in Tables 3 and 4, respectively. Of the 24 known WR stars in Westerlund 1 (23 excluding source S), 16 (15) are WN-type and 8 are WC-type, such that N(WC)/N(WN)$\sim$0.5 by number. As such, Westerlund 1 hosts 8% of the known Milky Way Wolf-Rayet population (van der Hucht 2006).

3.1 WN stars

He II 1.012μm/He I 1.083μm and He II 2.189μm/Brγ line ratios for selected Milky Way WN stars are presented in Fig. 5. The Y-band ratios broadly follow optical classification criteria, and

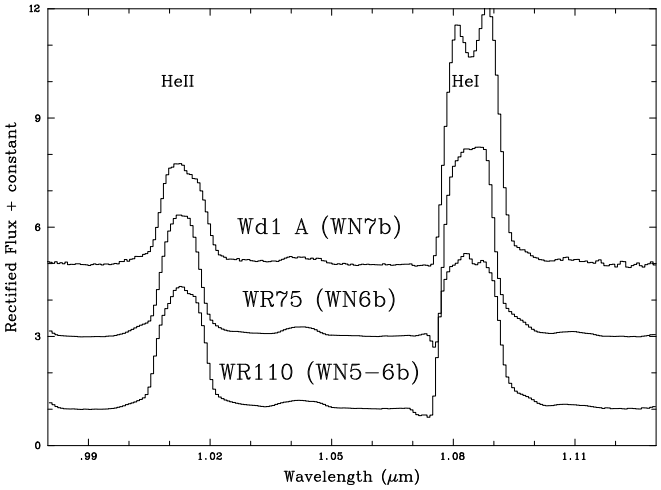

Figure 6. Spectroscopic comparison of Westerlund 1 source A (WN7b) with other broad-lined WN stars, WR110 (WN5-6b) and WR75 (WN6b), previously observed with NTT/SOFI (Homeier, priv. comm.).

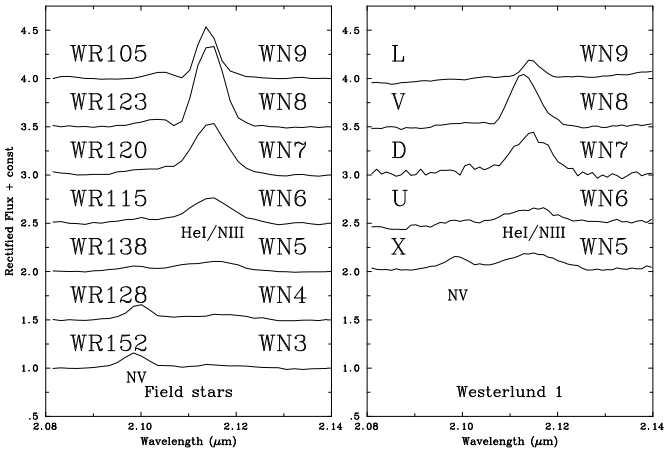

Figure 7. Spectral comparison of field weak-lined WN stars in the region of N V 2.100μm and He I/N III 2.115μm (from Crowther & Smith 1996) with selected Westerlund 1 stars

serve as excellent discriminators between WN4–6, WN7, WN8 and WN9 subtypes (see also Figer et al. 1997). For WN4–6 stars, He II/He I does not in general provide a unique spectral type, and instead groups stars according to strong, broad lined subtypes versus weak, narrow-lined subtypes (Hiltner & Schild 1966; Hamann et al. 1993). Smith et al. (1996) define broad lined WN stars as those for which FWHM (He II 4686Å) $\geqslant$ 30Å. Extending this definition to the near-IR, we may identify WN stars as strong/broad if FWHM (He II 1.012μm) $\geqslant$ 65Å and/or FWHM(He II 2.1885μm) $\geqslant$ 130Å, for which solely source A qualifies from Westerlund 1.

Individual stars are now discussed in turn, starting with the latest subtypes. He II 1.012μm is weak in star L, and potentially absent in S, indicating subtypes of WN9 and WN10-11: for these stars, respectively. Indeed, the weakness of He II 1.012μm in source S prevents an unambiguous classification, for which an alternate early B hypergiant classification (B0–1Ia$^+$) could be assigned. We favour a WN subtype due, in part, to the modest absolute magnitude inferred from our adopted distance in Sect. 4.

He II 1.012μm/He I 1.083μm indicators suggest WN8 subtypes for V and I, in agreement with earlier far-red spectral classifications. B, D, G and P have very similar near-IR line ratios, indicative of WN7 subtypes. For source W, the He II 2.189/Brγ ratio suggests a subtype of WN7 (Figer et al. 1997, Groh et al. 2006). However, the ratio of N III+He I 2.115μm/He II 2.189μm is 0.4 versus 0.7–1 in known Milky Way WN7 stars, such that we prefer WN6h (see later). Source A is unique amongst the WN stars in Westerlund 1 in displaying a strong, broad lined spectrum. This star is reminiscent of HD 165688 (WR110, WN5–6b) and HD 147419 (WR75, WN6b) except for an even stronger He I line strength such that we assign WN7b. 1μm NTT/SOFI spectroscopy of these stars are compared in Fig. 6, for which star A shows an apparent He I 1.083μm absorption feature, suggestive of an early B supergiant companion, which is also seen in He I 2.058μm.

WN5–6 subtypes are obtained for the other weak-lined WN stars. For these stars, spectral types are further refined using their spectral morphology in the 2.11μm region, which is a blend of N V 2.100μm and N III/He I 2.115μm. N V is relatively strong in WN3–4 stars and N III/He I is relatively strong in WN5–6 stars, as illustrated in Fig. 7, from which subtypes may be obtained, and as such this represents the best near-IR discriminator between such subtypes. Attempts at classification of broad-lined WN stars using this approach is not possible due to line blending.

Table 5. Quantitative near-IR classification of weak/narrow WN stars with FWHM(He II 1.012μm)$\leqslant$65Å. Values for strong/broad lined WN stars are shown in parenthesis.

Subtype	He II 1.012/ He I 1.083		N V 2.100/ He I/N III 2.115		He II 2.189/ Brγ	
WN3	>10		>2		1-3	
WN4	3-10	($>$0.8)	1-2	(blend)	1-3	($>$2)
WN5	1.5-3		0.2-1		1-3	
WN6	0.6-1.5	($>$0.5)	<0.25	(blend)	0.5-2.5	(1-2)
WN7	0.2-0.6	($>$0.5)		(blend)	0.5-1.2	(1-2)
WN8	0.07-0.2				0.1-0.4	
WN9	<0.07				$<$0.1	

Historically, the optical Pickering-Balmer decrement has been used to detect the presence of hydrogen in WN stars (Conti et al. 1983). Indeed, this is quantitatively included in the Smith et al. (1996) classification scheme, adopting o, (h), h for stars with no, weak or strong signatures of hydrogen. The question of hydrogen in WN stars is important, since from an evolutionary perspective, WN stars with/without hydrogen are identified as late/early-types, respectively, whilst the spectroscopic definition is dependent upon the observed degree of ionization.

For the WN5–6 stars, He II 2.189μm$\gg$Brγ, suggesting no hydrogen in most cases, i.e. WN5–6o. Stars J (WN5) and W (WN6) are obvious exceptions (lower panel in Fig. 5), from which we infer the presence of hydrogen in their atmospheres. For the WN7–9 stars, the presence of hydrogen can in principle be observed in the higher Paschen (n-3) or Brackett (n-4) series, relative to the alternating He II (n-6, n-8) series, although the contribution of hydrogenic He I lines to the Paschen/Brackett lines is significant in late WN stars. The observed He II 2.189μm/Brγ ratio for both I and V mimics the H-deficient WN8 star WR123 (Crowther et al. 1995) such that they are also expected to be strongly H-deficient. The same conclusions are reached for the WN7 stars in Westerlund 1 from comparison with WR120 (WN7o, Fig. 5). The situation is less clear for L and S, but we shall assume they contain hydrogen since all other WN9–11 stars are hydrogen rich. Of course, a detailed determination of abundances in WN stars await the result of

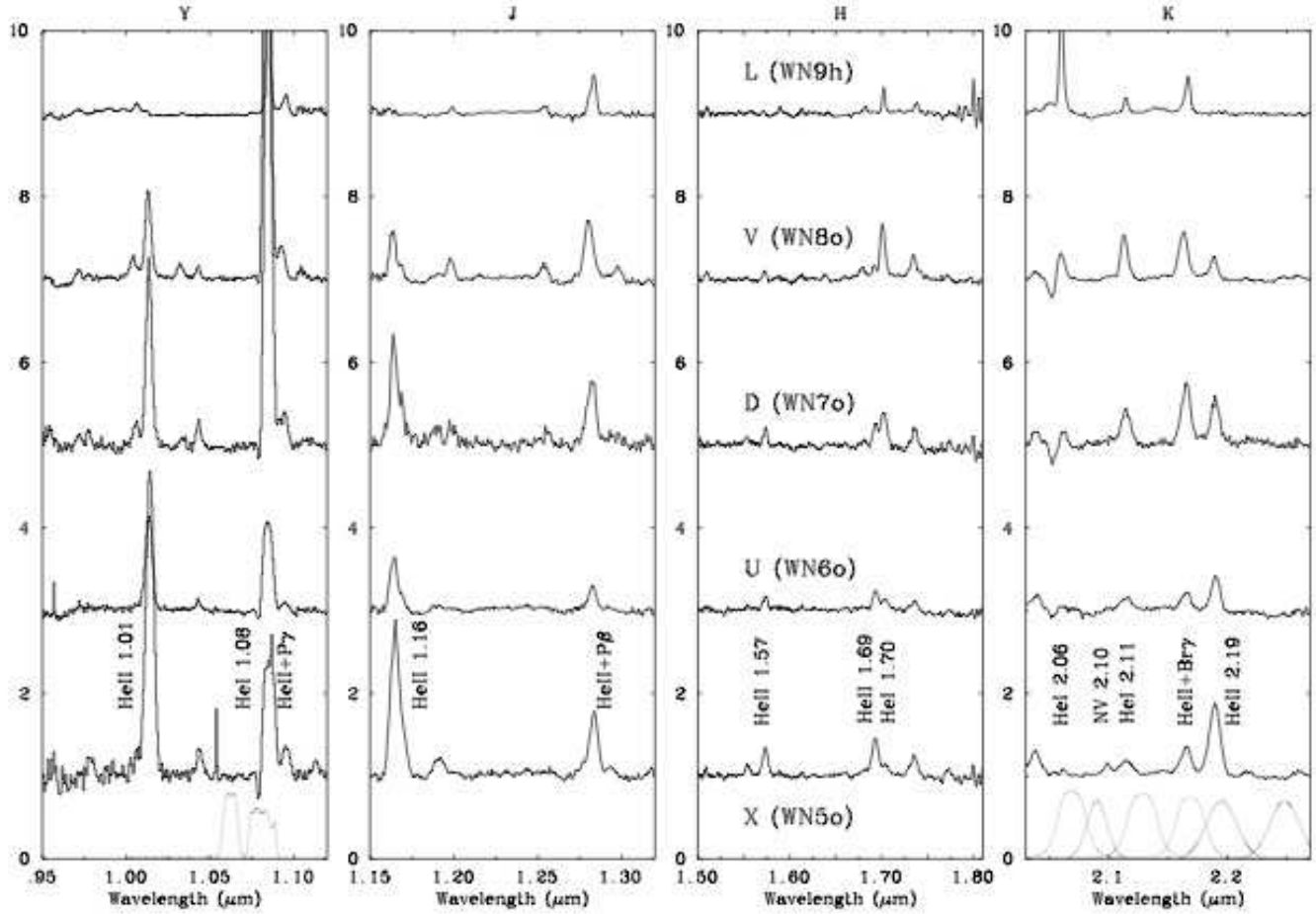

Figure 8. Near-IR spectroscopy of representative WN stars in Westerlund 1. NTT/SOFI Y-band and K-band interference filters used in this study are also indicated (dotted lines).

quantitative analysis, but our initial inspection suggests that 12/16 ($\sim$75%) of the WN stars in Westerlund 1 are highly deficient in hydrogen.

Representative near-IR spectra for Westerlund 1 WN stars are presented in Fig. 8, together with the Y-band and K-band interference filters used in Sect. 2. For reference, a summary of our quantitative near-IR classification for WN stars is presented in Table 5.

3.2 WC stars

The observed line ratios of C IV 2.076μm/C III 2.110μm and C III 0.971μm/C II 0.990μm are presented for Galactic WC stars in Fig. 9. As with WN stars, the near-IR line ratios permit one to discriminate between WC5–7, WC8 and WC9 stars. C II 0.990μm is uniformly weak in early subtypes, and C IV 2.076μm/C III 2.110μm remains fairly constant amongst WC5–7 subtypes (Figer et al. 1997), which is also true of other non-classification optical line ratios e.g. C IV 5805Å/C III 6740Å.

The K-band C IV/C III ratio serves as our primary classification diagnostic, from which a subtype of WC8 is inferred for source K. WC9 subtypes are indicated for the remainder, with measured C IV/C III ratios similar to known WC9 stars, with the possible exception of star N. This has the highest ionization of WC9 stars in Westerlund 1 from both the Y-band and K-band criteria, albeit hindered by a heavily dust diluted K-band spectrum, so it is necessary to consider whether WC8 or WC9 is most appropriate for source N, given that C II 1.78μm is also weak/absent, suggestive of a WC8 subtype.

Fortunately, a third near-IR diagnostic is available using the ratio C IV 1.191μm/C III 1.198μm, from which a conclusive classification is possible, as presented in Fig. 10. EW(C IV 1.191μm/C III 1.198μm)=1.5 for WR135 (WC8) and only $\sim$0.2 for WR75c and WR121 (WC9). This supports a WC9 subtype for star N since its C IV 1.191μm/C III 1.198μm ratio is 0.4. Indeed, red optical spectroscopy published by Negueruela & Clark (2005) reveals C III 5696Å $\gg$ C IV 5805Å from which an unambiguous WC9 subtype follows. In addition, C II λ7240 emission is prominent, in common with other optically visible WC9 stars.

Representative near-IR spectra for WC stars are presented in Fig. 11, for which three WC9 stars whose emission line spectra are progressively diluted by dust emission are included. Y-band and K-band interference filters used in Sect. 2 are also indicated. Our quantitative near-IR WC classification scheme is outlined in Table 6.

4 WESTERLUND 1 IN CONTEXT

In this section we use the Wolf-Rayet population of Westerlund 1 to estimate its global properties, namely distance, extinction and age. In addition, estimates of the current WR masses are presented.

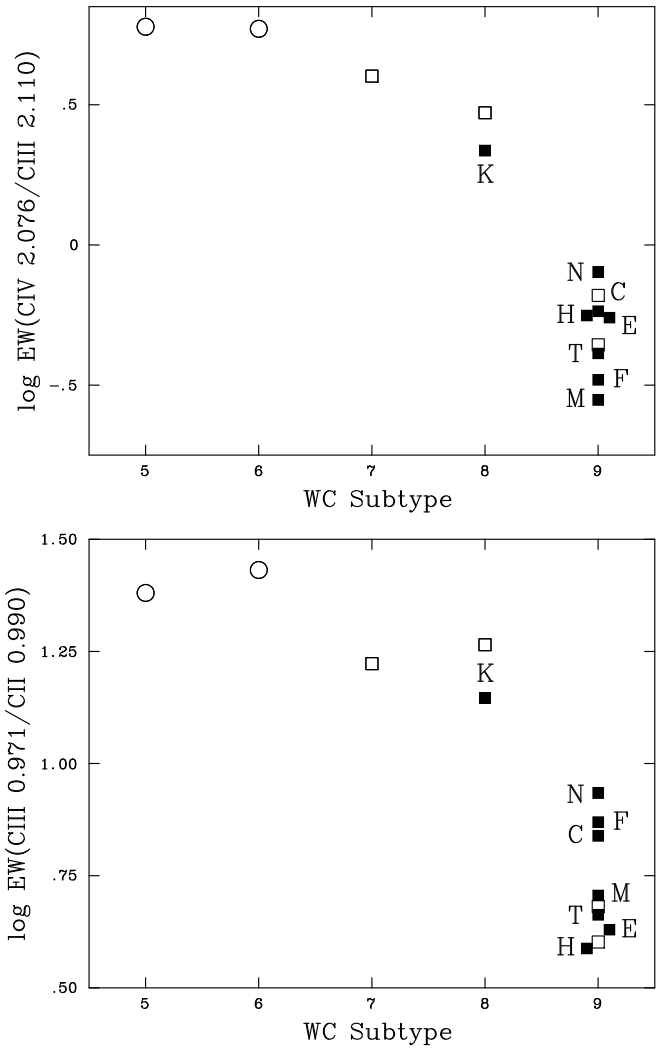

Figure 9. Near-IR diagnostic line ratios for Westerlund 1 WC stars (filled symbols) together with selected optically classified Milky Way stars (WR75c, 106, 111, 121, 135, 137, 154, open symbols) for which equivalent width measurements are from Howarth & Schmutz (1992), Eenens et al. (2001), Vacca et al. (2006) plus our own NTT/SOFI observations of WR75c. Early and late WC stars are indicated by circles and squares, respectively.

Table 6. Quantitative near-IR classification of WC stars

Subtype	C III 0.971/ C II 0.990	C IV 1.191/ C III 1.198	C IV 2.076/ C III 2.110
WC5–6	>15	> 4	>5
WC7	>15	2-4	>4
WC8	>10	0.8-2	1–4
WC9	<10	<0.8	< 1

4.1 Distance and extinction to Westerlund 1

We may used the Wolf-Rayet stars within Westerlund 1 to estimate its distance and foreground extinction, independently of yellow hypergiants, from which Clark et al. (2005) estimated $A_{\rm V}$=11.6 mag and an upper limit of 5.5 kpc. A revised calibration of absolute K-band magnitudes and intrinsic JHK colours for WN stars and non-dusty WC stars is presented in Appendix A, which is updated from

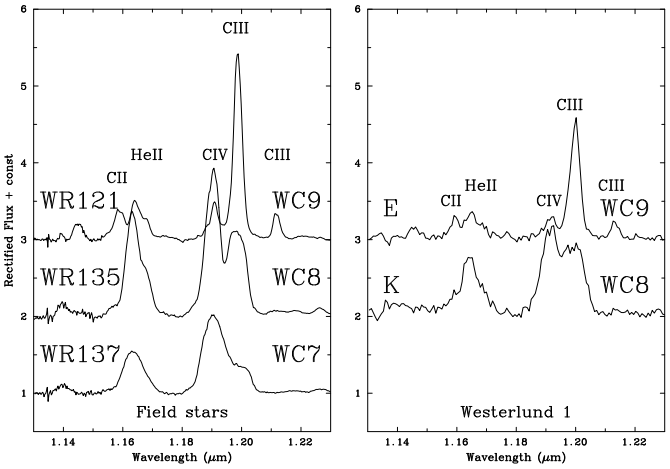

Figure 10. Spectral comparison of field WC stars in the region of C IV 1.19μm and C III 1.20μm (Vacca et al. 2006) with selected Westerlund 1 stars. These lines are hard to resolve in broad lined WC stars, typical of WC7 and earlier subtypes.

van der Hucht & Williams (2006) to include theoretical energy distributions. Generic theoretical near-IR colours should be reliable to $\pm$0.1 mag.

Interstellar K$_S$-band extinctions are estimated independently using the J–K$_S$ and H–K$_S$ colours for individual WN stars, adopting the Indebetouw et al. (2005) relationship between J, H and K$_S$ band extinctions, which are fairly line-of-sight independent, i.e.

$$A_{K_S} = 1.82^{+0.30}_{-0.23} E_{\rm H-K_S}$$

and

$$A_{K_S} = 0.67^{+0.07}_{-0.06} E_{\rm J-K_S}$$

We used the average of the two approaches for our adopted K$_S$-band extinction, $\overline{A_{K_S}}$.

We obtain a mean extinction of $\overline{A_{K_S}}$ = 0.96 mag for 16 WN stars, plus the non-dusty WC8–9 stars, from which mean H and J band extinctions of 1.5 mag and 2.4 mag follow, respectively, according to Indebetouw et al. (2005). We note the small standard deviation from which one may infer a rather uniform extinction towards Westerlund 1. Westerlund 1 does appear to suffer from an anomalous visual extinction law, as discussed by Clark et al. (2005), so $A_{\rm V}$ does not directly follow, without a determination of $R_{\rm V} = A_{\rm V}/E(B-V)$. For this reason we do not attempt to derive $A_{\rm V}$ from our near-IR observations. Nevertheless, the Galactic IR extinction law is independent of sight-line, such that our near-IR extinction estimate ought to be robust.

From our study, the mean distance modulus is 13.50 mag, corresponding to a distance of $\sim$5.0 kpc, somewhat higher than Brandner et al. (2006) who obtained 13.0$\pm$0.2 ($\sim$4.0 kpc). Indeed we wish to emphasise that Wolf-Rayet stars do not represent ideal distance calibrators, owing to the substantial scatter in their absolute magnitudes within individual subtypes. For example, –4.9 $\leqslant$ M$_{K_S}$ $\leqslant$ –6.8 for WN7–9 stars (Table A1). This scatter is the likely origin of the observed dispersion of σ=0.7 in the distance modulus for Westerlund 1. In addition, we shall show in Section 5 that several WN stars are thought to be binaries, affecting their role as distance calibrators. Fortunately, the contribution from an OB companion affects the K-band magnitude of the Wolf-Rayet star much less severely than in the V-band, since WR stars possess relatively

Table 7. Distance modulus and extinction to Westerlund 1 based upon the near-IR photometry of its member WN stars plus non-dusty WC stars (E and K). The K_S-band extinction is estimated using both the J–K_S and H–K_S colours, as discussed in the text. The average distance modulus (DM) equates to 5.0 kpc, in reasonable agreement to that obtained from yellow hypergiants by Clark et al. (2005)

Star	SpType	K_S	$A_{K_S}^{J-K_S}$	$A_{K_S}^{H-K_S}$	$\overline{A_{K_S}}$	K_S - $\overline{A_K}$	DM
A	WN7b	8.37	0.89	0.85	0.87	7.50	12.27
B	WN7o	9.18	0.99	0.91	0.95	8.23	14.15
D	WN7o	9.61	1.19	1.07	1.13	8.48	14.40
G	WN7o	9.28	1.23	1.05	1.14	8.14	14.06
I	WN8o	8.86	1.19	1.09	1.14	7.72	13.64
J	WN5h	9.70	1.11	0.80	0.95	8.75	13.15
L	WN9h:	7.19	1.10	0.76	0.93	6.26	12.18
O	WN6o	9.45	0.81	0.67	0.74	8.71	13.12
P	WN7o	9.26	1.04	0.84	0.94	8.32	14.25
Q	WN6o	10.00	0.92	0.93	0.92	9.08	13.48
R	WN5o	10.26	0.87	0.76	0.82	9.44	13.85
S	WN10-11h	8.29	0.81	0.71	0.76	7.53	14.40
U	WN6o	9.20	0.82	0.65	0.74	8.46	12.87
V	WN8o	8.76	1.17	1.00	1.08	7.68	13.60
W	WN6h	10.04	1.15	1.00	1.08	8.96	13.37
X	WN5o	10.25	1.18	1.22	1.20	9.05	13.46
K	WC8	9.53	0.98	0.89	0.94	8.59	13.24
E	WC9	8.29	0.89	0.98	0.94	7.35	
					0.96		13.50
					$\pm$0.14		$\pm$0.66

flat spectral energy distributions with respect to O stars, due to the free-free continuum emission from their winds.

The distance to Westerlund 1 may confidently be assumed to be $5^{+0.5}_{-1.0}$ kpc unless binarity systematically affects the present results. For an assumed Solar galactocentric distance of 8.5 kpc, this places Westerlund 1 at a galactocentric distance of $4.2^{+0.75}_{-0.35}$ kpc, i.e. similar to the outer edge of the Galactic bar, which also extends to 4.4 $\pm$ 0.4 kpc (Benjamin et al. 2005). This location may prove significant for the formation of a $10^5 M_\odot$ cluster within the Milky Way.

The Galactic oxygen metallicity gradient has recently been estimated from optical recombination lines by Esteban et al. (2005) revealing $\Delta \log$(O/H) = –0.044 $\pm$ 0.010 dex kpc^{-1}, such that the metallicity of Westerlund 1 is anticipated to be moderately oxygen-rich, exceeding that of the Orion Nebula by 60%, i.e. $\log$ (O/H) + 12 $\sim$ 8.87.

4.2 Age

Clark et al. (2005) estimated a mass of $10^5 M_\odot$ for Westerlund 1 on the basis of an age of 4–5 Myr and a Kroupa initial mass function (IMF). This choice of IMF appears to be borne out by recent VLT/NACO imaging (Brandner et al. 2006), whilst the age was selected on the basis of the simultaneous presence of WR stars, red supergiants and yellow hypergiants within the cluster. Red supergiants are predicted after 4 Myr, whilst WR populations decline rapidly after 5 Myr, especially those based on single star evolutionary models. Definitive near-IR studies of the main sequence stars in Westerlund 1 are ongoing, although late O stars appear to be present, such that the turn-off age is in broad agreement with 4–5Myr.

The ratio of the red supergiants and yellow hypergiants to the number of WR stars in Westerlund 1, N(RSG + YHG)/N(WR) = 8/24 = 1/3, including the recently identified red supergiant W75 (Clark, priv. comm.). In principle, this should provide robust constraints upon its age. Vanbeveren et al. (1998) show the lifetimes of these phases versus initial mass for single stars, suggesting a negligible red supergiant lifetime for initial masses in excess of 40 $M_\odot$ and a decreasing WR lifetime below this initial mass. According to Eldridge & Tout (2004) models, the observed ratio is best reproduced at an age of 4.5–5.0 Myr. As we shall see, stellar evolution models poorly predict individual WR subtype distributions. Nevertheless, predicted total WR populations are rather well matched, validating our present approach.

4.3 WR stars in Milky Way clusters

From membership of WR stars in open clusters, Schild & Maeder (1984) and Massey et al. (2001) investigated the initial masses of WR stars empirically, from the membership of WR stars in Milky Way clusters, to which we can now add Westerlund 1, which hosts more WR stars than all the other optically visible cluster combined. A compilation of optically visible Milky Way clusters containing WR stars is shown in Table 8, where we have derived the highest (initial) mass OB star for each cluster following the methodology of Massey et al. (2001), except that we take account of the revised spectral type-$T_{\rm eff}$ calibration of Martins, Schaerer & Hillier (2005) for O stars, Crowther, Lennon & Walborn (2006) for B supergiants, plus the high mass-loss Meynet et al. (1994) Solar metallicity isochrones. Highly reddened clusters, such as the Quintuplet cluster at the Galactic Centre and SGR 1806-20 are also omitted. To illustrate our approach, we list parameters for the highest initial mass OB stars within each cluster in Appendix B.

Hydrogen-rich WN stars are observed in young massive clusters, indicating initial masses in excess of $\geqslant 60 - 110 M_\odot$), where the effect of uncertainties in distance moduli are shown for clusters within the Car OB1 association (Humphreys 1978; Massey & Johnson 1993). Indeed, these are believed to be core-H burning massive O stars with strong winds (Langer et al. 1994; Crowther et al. 1995). Lower mass progenitors of $\geqslant 40 M_\odot$ are indicated for WC9 stars together with mostly weak-lined hydrogen free WN5–6 stars based primarily upon their large population in Westerlund 1, plus Sand 5 (WO) in Berkeley 87. Some early WN progenitors appear to originate from lower mass stars, suggesting a low mass cutoff to the formation of a WR star no higher than 20–25$M_\odot$ at Solar metallicity.

5 WR PROPERTIES

5.1 Binarity

From the known WR sample within Westerlund 1, none have been subject to photometric or spectroscopic monitoring, hindering efforts towards establishing a binary fraction. OB companions for Milky Way WR stars have typically been suspected from the presence of photospheric absorption lines in blue optical spectroscopy, which is unrealistic for highly reddened Westerlund 1 members. Nevertheless, two methods are at our disposal with regard to investigating WR binarity.

First, persistent and episodic dusty WC stars are considered to be in binary systems with OB companions (e.g. WR104, Tuthill et al. 1999). Hydrogen from the OB star and carbon from the WC star provide suitable ingredients, whilst their wind interaction regions

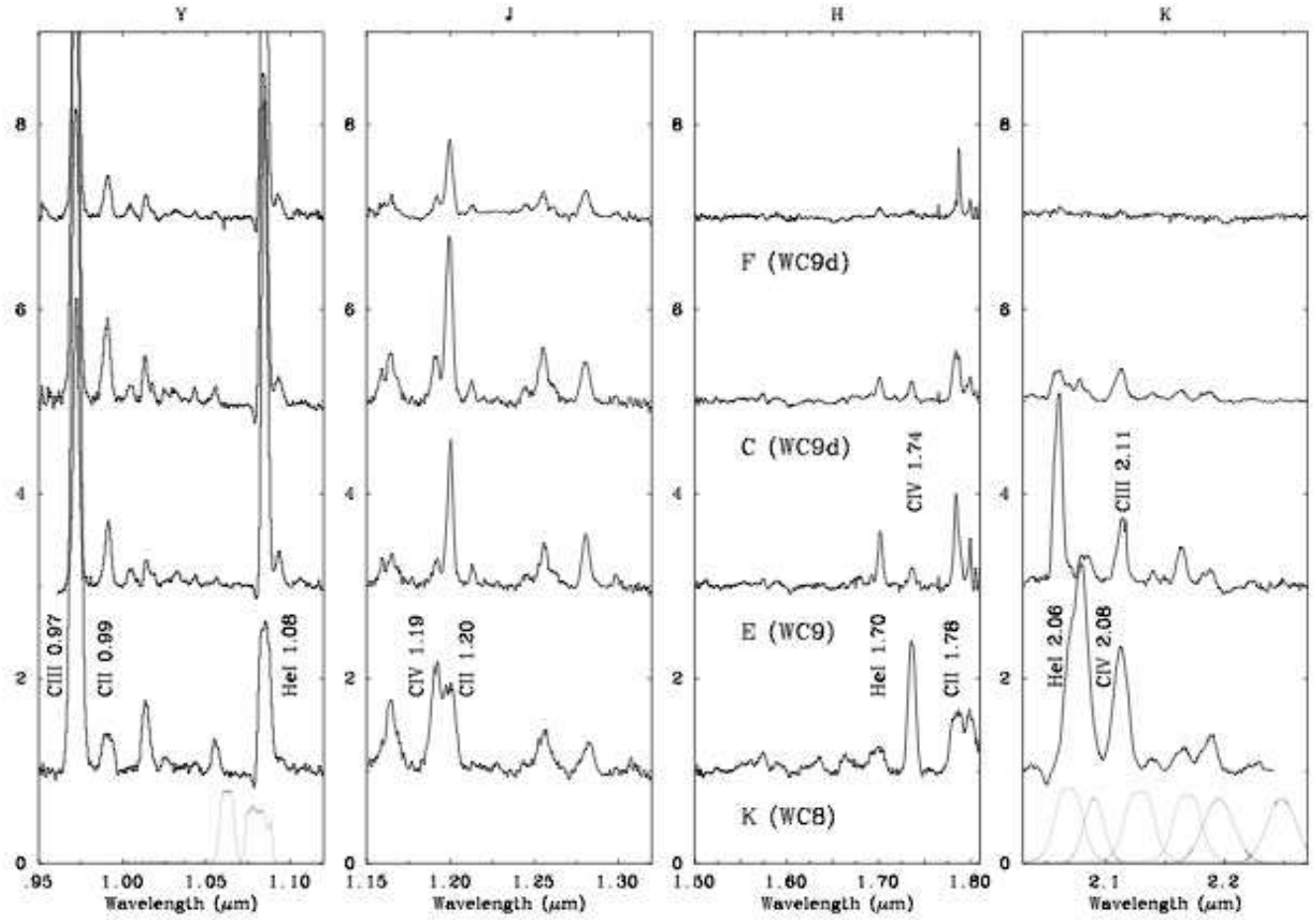

Figure 11. Near-IR spectroscopy of representative WC stars in Westerlund 1. NTT/SOFI Y-band and K-band interference filters used in this study are also indicated (dotted lines).

may provide shielding from their intense UV radiation fields plus the necessary high densities (e.g. Crowther 2007).

With regard to the presence or absence of dust within WC stars, T, N, C, H, M and F all reveal a strong near-IR excess with respect to the normal stellar energy distribution (recall Fig. 4) indicative of hot dust (Williams et al. 1987). K-band spectral features are strongly diluted due to the dust with respect to shorter wavelengths where the contribution of dust is reduced (Fig. 11). Consequently at least 75% of the WC stars are likely to be binary systems from the presence of dust emission.

For stars K (WC8) and E (WC9) the situation is less clear. The ratio of C III 2.110μm/0.971μm in star K is identical to the non-dusty WC8 star WR135, such that K does not appear to be forming dust. Similarly, the ratio of C III 2.110μm/0.971μm in star E is similar to the non-dusty WC9 star WR75c (Hopewell et al. 2005). In addition, the *Spitzer* IRAC 3.6–8μm colours of star E presented in Table 2 are similar to non-dusty WN stars, so it too is probably not forming dust. Of course, the absence of dust emission does not exclude binarity, since relatively short period late-type WC binaries (e.g. γ Vel, WC8+O) are known not to form dust. Consequently, the WC binary fraction could be as high as 100%.

Second, WR stars in binary systems with a massive companion are often hard X-ray emitters (e.g. V444 Cyg, WN5+O), produced in the shocked region where their winds collide. Most single OB and WN stars are relatively soft in X-rays (kT = 0.5 keV, Skinner et al. 2002), whilst those in close binaries additionally possess a harder X-ray component of $\sim$2–3 keV, presumably from the shocked wind-wind collision zone.

Westerlund 1 has been observed with *Chandra*, from which Skinner et al. (2006) and Clark et al. (2006) have matched strong, hard X-ray sources to the known Wolf-Rayet population. WN stars A, B and L, plus the dust forming WC9 star F possess strong ($L_X \geqslant 10^{32}$ erg s^{-1}), hard X-ray emission with a characteristic temperature of 2–3keV, plus radio detections. In addition, several other WN stars possess hard X-ray components, albeit with typically lower L_X and no radio detections, namely D, W, G, R, O and U. Consequently, 3 out of 16 of the WN stars are firm binary candidates, whilst another 6 are possible WN binaries from the hardness of their X-ray colours. Recall several He I lines in star A exhibit central P Cygni absorption, which is also suggestive of an early type companion. Note the weak emission line strength of star B led Negueruela & Clark (2005) to suggest that this was a binary.

Therefore, a significant fraction of the WR stars in Westerlund 1 appear to be members of close, massive binary systems, with a minimum of 3/16 WN stars (X-rays) plus 6/8 WC stars (dust, X-rays), i.e. $\geqslant$38% of the total WR content, or more likely a total of 9/16 WN stars plus 6/8 WC stars i.e. $\geqslant$62% of the total WR content, including the other hard X-ray sources. However, to reiterate, our present observations do not exclude a binary fraction of 100%.

Table 8. Optically visible Milky Way clusters hosting WR stars, sorted in order of decreasing initial mass of the most massive OB star according to Meynet et al. (1994) Solar metallicity isochrones. Our approach updates that of from Schild & Maeder (1984) and Massey, DeGioia-Eastwood & Waterhouse (2001) to take account of the revised OB temperature calibrations of Martins et al. (2005) and Crowther et al. (2006). We include an estimate for the cluster turn-off mass for Westerlund 1

Cluster	DM (mag)	Ref	Age (Myr)	Mass ($M_\odot$)	WR Cat	Star	Subtype
Cyg OB2	11.2	5	2±0.2	110:	WR144		WC4
NGC 3603	14.25	2	1.3±0.3	105	WR43a,b,c	HD 97950A1,B,C	WN5ha
Pismis 24	12.0	8	1.8±0.2	105	WR93	HD 157504	WC7
Trumpler 16	12.1,12.5	1,6	1.5±0.5	80,105	WR25	HD 93162	WN6ha
Havlen-Moffat 1	12.0	8	2.2±0.5	75	WR87	LSS 4064	WN7h
					WR89	LSS 4065	WN8h
NGC 6231	11.5	3	2.7±0.5	75	WR78	HD 151932	WN7h
Collinder 228	12.1,12.5	1,6	2.5±0.5	65,100	WR24	HD 93131	WN6ha
Trumpler 27	12.0	8	3.5±1.0	50	WR95	He3 1434	WC9
Westerlund 2	14.5	4	2.6±0.2	50	WR20a		WN6ha+WN6ha
Berkeley 87	11.0	8	3±1.0	50	WR142	Sand 5	WO2
Westerlund 1	13.5	10	4.5±0.5	(40::)	WR77e,q,sd	J,R,X	WN5o,h
					WR77a,s,sa,sb	O,Q,U,W	WN6o,h
					WR77d,j,o,r,sc	A,B,D,G	WN7b,o
					WR77c,h	I,V	WN8o
					WR77k	L	WN9
					WR77f	S	WN10-11:
					WR77g	K	WC8
					WR77b,i,l,m,n,p,aa	C,E,F,H,M,N,T	WC9
Pismis 20	12.7	8	4.5:	40	WR67	LSS 3329	WN6
NGC 6871	11.65	7	3.2±0.7	40	WR133	HD 190918	WN5+O9.5Ia
Berkeley 86	11.4	7	3.7±1	35	WR139	V444 Cyg	WN5+O6
Bochum 7	13.45	9	2.8±0.5	35	WR12	LSS 1145	WN8h
Ruprecht 44	13.35	8	3.5	22	WR10	HD 65865	WN5h
Markarian 50	12.8	8	7–10	18	WR157	HD 219460B	WN5

(1) Humphreys 1978; (2) Moffat 1983; (3) Perry et al. 1991; (4) Moffat et al. 1991; (5) Massey & Thompson 1991; (6) Massey & Johnson 1993; (7) Massey et al. 1995; (8) Massey et al. 2001; (9) Corti et al. 2003; (10) this study

5.2 Current stellar masses

There is a well known mass-luminosity relationship for H-deficient WR stars (e.g. Schaerer & Maeder 1992) from which we may estimate current masses. For our derived distance modulus of 13.5 mag, plus individual K_S-band extinctions, we may determine the absolute K_S-band magnitude M_{K_S}, which is representative of the stellar continuum, except for the dusty WC stars. Quantitative analysis of individual WR stars in Westerlund 1 is presently in progress. Until such results are available, calibrations for individual subtypes (e.g. Crowther 2007) need to be applied. WR bolometric corrections are typically quoted for the v-band, such that theoretical $(v - K_S)_0$ WR spectral energy distribution colours also need to be used (see Table A1). Results from this approach are presented in Table 9 and suggest current WR masses in the range 10–18$M_\odot$ with 14$M_\odot$ on average. These are fairly typical of Milky Way WR masses, as deduced from binary orbits (e.g. Crowther 2007).

We have excluded the dusty WC9 stars from this sample, since dust contributes to their K_S-band magnitudes, such that bolometric magnitudes and masses would otherwise be seriously overestimated. If we were to apply dust-free WC9 intrinsic colours from Table A1 for the six WC9d stars to derive A_{K_S}, we would obtain –7.0 $\leqslant M_{K_S} \leqslant$ –9.1 mag. Application of standard bolometric corrections would naturally yield unrealistic current masses in the range 30–180 $M_\odot$.

Consequently, great care has to be taken when using near-IR observations of dusty WC stars as indicators of distance or stellar luminosity. For example, Eikenberry et al. (2004) justify a large distance towards the SGR 1806-20 cluster partially on the basis of M_{K_S} = –8.6 mag for their 'star B' with a WC9d spectral type. Weak K-band spectral features are observed in this star, one would expect only moderate dust contamination, i.e. a K_S-band absolute magnitude close to –7 mag, and so a near distance, broadly consistent with that suggested by Cameron et al. (2005).

6 SINGLE VERSUS BINARY EVOLUTION

6.1 Single star models

We have compared the number, and subtype distribution, of WR stars in Westerlund 1 with those predicted by the evolutionary synthesis model Starburst99 (Leitherer et al. 1999), assuming Solar metallicity, an instantaneous burst, a Kroupa IMF and an upper mass limit of $\sim 120M_\odot$. Two Geneva group evolutionary models may be used, with standard or enhanced mass-loss rates for individual stars (Schaller et al. 1992; Meynet et al 1994). The latter is normally preferred, since rotation is neglected in such models. The total WR population is reasonably well reproduced, particularly for the enhanced mass-loss case, although the ratio N(WC)/N(WN) is far too high in all cases. Indeed, WN stars are predicted to be H-rich (WNL from an evolutionary definition), in contrast to the observed H-poor WN stars within Westerlund 1. The number of O stars in Westerlund 1 – predicted to be N(O)=150–320 for an age of 4–

Table 9. Mass estimates of WR stars for our deduced distance modulus of 13.5 mag, plus bolometric corrections from the calibration of Crowther (2007) and theoretical colours from Table 8, together with the mass-luminosity relation for H-free WR stars (Schaerer & Maeder 1992).

Star	Sp Type	$M_{\rm K_S}$ mag	$M_{\rm bol} - M_v$ mag	$M_v - M_{\rm K_S}$ mag	$M_{\rm bol}$ mag	M $M_\odot$
A	WN7b	–6.0	–4.1	0.6	–9.5	18.3
B	WN7o	–5.3	–3.7	–0.2	–9.2	15.3
D	WN7o	–5.0	–3.7	–0.2	–8.9	13.3
G	WN7o	–5.4	–3.7	–0.2	–9.3	16.0
I	WN8o	–5.8	–3.2	–0.2	–9.2	15.3
J	WN5h	–4.8	–4.2	–0.2	–9.1	
L	WN9h:	–7.2	–2.8	–0.2	–10.3	
O	WN6o	–4.8	–4.2	–0.2	–9.2	14.9
P	WN7o	–5.2	–3.7	–0.2	–9.1	14.5
Q	WN6o	–4.4	–4.2	–0.2	–8.8	12.3
R	WN5o	–4.1	–4.2	–0.2	–8.4	10.1
S	WN10-11h:	–6.0	(–2.2)	(0.0)	(–8.2)	
U	WN6o	–5.0	–4.2	–0.2	–9.4	17.2
V	WN8o	–5.8	–3.2	–0.2	–9.2	15.8
W	WN6h	–4.5	–4.2	–0.2	–8.9	
X	WN5o	–4.5	–4.2	–0.2	–8.8	12.4
E	WC9	–6.1	–3.0	–0.1	–9.2	15.4
K	WC8	–4.9	–4.1	0.5	–8.5	10.5

5Myr – awaits the completion of an ongoing near-IR spectroscopic survey.

Table 10 presents predicted WR subtype distributions from single star evolution at ages of 4–5Myr from Eldridge (2006, priv. comm.), based upon Solar metallicity models presented by Eldridge & Tout (2004), in which rotation is neglected, whilst convective overshooting is considered. The Eldridge & Tout models are favoured with respect to evolutionary models from Meynet et al. (1994) since their predicted N(WC)/N(WN) ratio is less extreme, in better agreement with the Westerlund 1 Wolf-Rayet population. However, theoretical N(WN H-rich)/N(WN H-poor) ratios remain larger than those observed in Westerlund 1. Note that for an age of $\sim$4.5Myr, the WR progenitor mass lies in the range 40–55$M_\odot$. As a result, it is likely that the progenitor of the pulsar identified by Muno et al. (2006) had an initial mass in excess of $50M_\odot$.

Rotation is, thus far, neglected in such synthesis models, but has recently been considered for individual evolutionary models by Meynet & Maeder (2003), from which some conclusions may be inferred. The impact of rotational mixing is to extend the WR lifetime and reduce the mass threshold for WR formation, from 37 to $22M_\odot$ for nominal initial rotation rates at Solar metallicity. This has the effect of increasing the N(WR)/N(O) number ratio, and decreasing the predicted N(WC)/N(WN) ratio. This would improve the comparison with Westerlund 1. However, WN stars in Westerlund 1 appear to be largely H-poor, in contrast with the extended H-rich WN phases and diminished H-poor WN phases predicted by rotating models (Meynet & Maeder 2003).

6.2 Binary evolution

Close binary evolution has been neglected thus far, so we additionally need to consider this formation channel for WR stars, in particular given the high density within the cluster core. We know of at least one pulsar in Westerlund 1 which has probably been formed as a result of massive close binary evolution (Muno et al. 2006).

Table 10. WR number ratios predicted by single and binary evolutionary models at Solar metallicity from Eldridge (2006, priv. comm.), based upon models presented by Eldridge & Tout (2004) in which rotational mixing is neglected, versus the observed WR population in Westerlund 1. Similar results for single stars are obtained by Meynet et al. (1994). Eldridge & Tout (2004) define an upper limit to a H-poor WN star as X(H)=0.1%, by mass, whilst the approximate observational limit is $\sim$5%.

Age Myr	N(WN H-rich)/ N(WN H-poor)	N(WC)/ N(WN)	Mass Range $M_\odot$
	Single stars		
4–4.5	0.8	1.5	45–60
4.25–4.75	1.2	2.4	40–55
4.5–5.0	1.5	1.6	38–45
	Binary stars		
4.0–4.5	2.0	0.9	
4.25–4.75	1.1	1.4	
4.5–5.0	0.7	1.1	
	Westerlund 1		
	0.25	0.5	

Theoretically, close binary evolution causes the premature loss of the H-rich mantle during Roche lobe overflow or common envelope evolution, leading to an extended H-rich WN phase. Unfortunately, predictions greatly depend upon a large number of additional parameters, notably the initial binary fraction, their mass ratio and their initial period distribution. Nevertheless, the predicted WR subtype distribution for close binary is presented in Table 10, which improves the predicted N(WC)/N(WN) ratio, but does not resolve the discrepancy.

The location of two WR stars far from the central cluster of Westerlund 1 (T and N) suggests either an ejection via dynamical interactions within the cluster at an early phase, or the recoil following a supernova (SN) explosion within a massive binary system. Both lie 4.5 arcmin from the cluster, which equates to a projected distance of $\sim$7 pc, suggesting velocities of $\sim$1.5–6 km/s for ejection 1–4 Myr ago. However, both systems are dust forming WC9 stars, suggesting binary OB companions. Neither method of ejecting the WR from the cluster core outlined above would naturally explain such a scenario – dynamical interactions naturally favour ejection of single stars, whilst a runaway nature would require that the companion has already undergone a SN explosion.

7 CONCLUSIONS

We present interference filter Y- and K-band imaging and follow up near-IR spectroscopy in order to identify the complete WR population within Westerlund 1. Our results are as follows:

(i) Four WR stars in Westerlund 1 are newly confirmed here, with nomenclatures of U, V, W, X following Clark & Negueruela (2002), Negueruela & Clark (2005) and Hopewell et al. (2005), bringing the total number of WR stars to 24. Of these, U and V were previously discovered from optical spectroscopy (Negueruela, 2005, priv. comm.), whilst U, W and X have been independently reported by Groh et al. (2006). Indeed, our photometric approach is similar to Groh et al. (2006) except that we probe deeper in the Y-band and cover a larger field, but neglect the He II 1.0124μm filter.

(ii) Intermediate resolution JHK spectroscopy for all 24 WR

stars in Westerlund 1 are presented. We present a quantitative near-IR classification scheme for WN and WC stars, calibrated using line strengths measured in optically visible field WR stars. From our sample, 16 WN stars are fairly evenly divided between mid (WN5–6) and late ($\geqslant$WN7) subtypes, whilst all 8 WC stars are late subtypes (7/8 are WC9 stars). The majority ($\sim$75%) of early and late WN stars are H-poor, as estimated from the strength of Paschen/Brackett lines. Amongst the WN stars, solely star A shows a strong, broad line spectrum (WN7b), which is indicative of a dense, fast stellar wind.

(iii) Dominant late WC populations, such as those in Westerlund 1 are well known in metal-rich regions such as the inner Milky Way (Hopewell et al. 2005) and M83 (Hadfield et al. 2005). Early subtypes dominate in metal-poor regions. The reason for this dichotomy appears to be, at least in part, due to the sensitivity of WC spectral classification to (metallicity-dependent) wind strength (Crowther et al. 2002), rather than elemental abundance differences.

(iv) From a total of eight WC stars within Westerlund 1, six contain hot dust, which has the effect of strongly diluting the K-band spectral features with respect to shorter wavelengths - e.g. C III 2.11μm/0.971μm = 0.42 for the only apparent non-dusty WC9 star (E) versus 0.02 for star F. 2μm narrow-band surveys presently underway to identify visibly obscured WR stars in the Milky Way (e.g. Homeier et al. 2003ab) will not be so sensitive to such dusty WC stars due to the dilution of their emission lines by dust continuum. Instead, dust forming WC stars will most easily be detected at shorter wavelengths where their stellar signature is much more prominent, or via their hot dust signatures from near and mid-IR photometry.

(v) It is widely believed that dust formation in WR stars requires the presence of an OB companion, such that most WC stars within Westerlund 1 are binaries. The presence of hard X-ray emission from a subset of WN stars (Skinner et al. 2006; Clark et al. 2006) indicates a minimum WR binary fraction of $\sim$38% in Westerlund 1, or more likely 62%. Indeed, our present observations do not exclude a WR binary fraction of 100%.

(vi) We apply an absolute K-band calibration for our (non-dusty) WR stars to estimate the distance and extinction, revealing $\sim$5.0 kpc and A_{K_S}=0.96 $\pm$0.14 mag, in reasonable agreement with previous studies based upon yellow hypergiants and pre-main sequence stars (Clark et al. 2005; Brandner et al. 2006). WC9 stars were excluded from our calibration since non-dusty WC9 stars were not previously known within optically visible clusters (van der Hucht & Williams 2006). Applying our Westerlund 1 distance to the only non-dusty WC9 star (star E), suggests M_{K_S} = –6.2 mag (the remainder span –7.0 to –9.1 mag).

(vii) For an assumed Solar galactocentric distance of 8.5 kpc, Westerlund 1 lies at a galactocentric distance of $4.2^{+0.75}_{-0.35}$ kpc, i.e. similar to the outer edge of the Galactic bar (Benjamin et al. 2005). This location may prove significant for the formation of a $10^5 M_\odot$ cluster within the Milky Way. Based on the Esteban et al. (2005) Milky Way oxygen metallicity gradient, Westerlund 1 is anticipated to be moderately oxygen-rich, exceeding that of the Orion Nebula by 60%, i.e. $\log$ (O/H) + 12 $\sim$8.87.

(viii) For the hydrogen-deficient, non-dusty WR stars we have applied model atmosphere bolometric corrections and intrinsic visual to JHK$_S$ colours to provide estimates of stellar luminosities, from which masses follow using the mass-luminosity relation of Schaerer & Maeder (1992). We estimate current masses of 10–18$M_\odot$, typical of binary orbit deduced masses for Milky Way Wolf-Rayet stars (e.g. Crowther 2007).

(ix) We provide revised mass limits for WR progenitors in other optically visible Milky Way clusters, updated from Massey et al. (2001). We adopt revised OB spectral type–temperature calibrations and apply Solar metallicity isochrones from Meynet et al. (2004). Westerlund 1 more than doubles the known statistics, and includes subtypes not previously covered. The observed ratio N(WR)/N(RSG + YHG) $\sim$3 for Westerlund 1 suggests an age of $\sim$4.5–5.0 Myr, from comparison with evolutionary models, such that the WR stars are descended from stars of initial mass $40-55 M_\odot$ with potential implication for a higher progenitor mass for the pulsar recently observed in Westerlund 1 (Muno et al. 2006). Consequently, approximately 75% of the WR progenitor mass has been removed due to stellar winds or close binary mass-transfer.

(x) Comparisons between the observed WR population in Westerlund 1 and evolutionary models for rotating/non-rotating Solar metallicity stars is rather poor, in the sense that the observed ratios of N(WC)/N(WN) and N(WN H-rich)/N(WN H-poor) are rather lower than predicted, for both single and binary models.

We intend to follow up the present observational study with quantitative analysis of the WR population in Westerlund 1 from which we will be able to extract more reliable abundances, stellar luminosities and current masses, plus wind properties, with which to better test current evolutionary predictions for single and binary massive stars.

ACKNOWLEDGEMENTS

Thanks to Cedric Foellmi for obtaining jittered J, H and K$_S$ band NTT/SOFI images of Westerlund 1, to Nicole Homeier for providing NTT/SOFI spectroscopy of comparison broad-lined WN stars, to John Eldridge for generating comparisons with evolutionary predictions, and to Jose Groh for distributing his preprint prior to publication. Malcolm Currie provided invaluable help with applying ORAC-DR to ESO datasets. We appreciate critical comments from the referee, Peredur Williams, which helped improve several aspects of this paper. PAC acknowledges financial support from the UK Royal Society. IN is a researcher of the programme *Ramón y Cajal*, funded by the Spanish Ministerio de Educación y Ciencia (MEC) and the University of Alicante, with partial support from the Generalitat Valenciana and the European Regional Development Fund (EDRF/FEDER). This research is partially supported by the MEC under grant AYA2005-00095. This publication makes use of data products from the Two Micron All Sky Survey, which is a joint project of the University of Massachusetts and the Infrared Processing and Analysis Center/California Institute of Technology, funded by the National Aeronautics and Space Administration and the National Science Foundation

REFERENCES

Barlow M.J., Smith L.J., Willis A.J., 1981, MNRAS 196, 101
Benjamin R.A., Churchwell E., Babler B.L. et al. 2003, PASP 115, 953
Benjamin R.A., Churchwell E., Babler B.L. et al. 2005, ApJ 630, L149
Bohannan B., Crowther P.A., 1999, ApJ 511, 374
Brandner W., Clark J.S., Waters R., Stolte A., Negueruela I. 2006, A&A in preparation
Cameron P.B., Chandra P., Ray A. et al. 2005, Nat 434, 1112
Clark J.S., Negueruela, I., 2002, A&A 396, L25

Clark J.S. Negueruela I., Crowther P.A., Goodwin S.P., 2005, A&A 434, 949
Clark J.S., Muno M.P., Negueruela I., Dougherty S.M., Crowther P.A., Goodwin S.P. 2006, A&A to be submitted
Conti P.S., Leep M.E., Perry D.N., 1983, ApJ 268, 228
Corti M., Niemela V., Morrell N., 2003 A&A 405, 571
Crowther P.A., 2007, ARA&A in preparation.
Crowther P.A., Smith L.J., 1996, A&A 305, 541
Crowther P.A., Smith L.J., 1997, A&A 320, 500
Crowther P.A., Dessart L. 1998 MNRAS 296, 622
Crowther P.A., Hillier D.J., Smith L.J., 1995, A&A 293, 403
Crowther P.A., De Marco O., Barlow M.J., 1998, MNRAS 296, 367
Crowther P.A., Dessart L., Hillier D.J. et al. 2002, A&A 392, 653
Crowther P.A., Lennon, D.J., Walborn N.R. 2006, A&A 446, 279
Dessart L., Crowther P.A., Hillier D.J. et al. 2000, MNRAS 315, 407
Economou F., Jeness T., Currie M., Adamson A., Allan A., Cavanagh, B., 2004, ORAC-DR 4.1-0, Starlink User Note 230.6, Rutherford Appleton Laboratory
Eenens P.R.J., Williams P.M., Wade R., 1991, MNRAS 252, 300
Eikenberry S.S., Matthews K., LaVine J.L. et al. ApJ 616, 506
Eldridge J.J., Tout C.A., 2004, MNRAS 353, 87
Esteban C., Garcia-Rojas J., Peimbert M., Peimbert A., Ruiz M.T., Rodriguez M., Carigi L., 2005, ApJ 618 L95
Figer D.F., McLean I.S., Najarro F., 1997, ApJ 486, 420
Groh J.H., Damineli A., Teodoro M., Barbosa C.L. 2006, A&A in press (astro-ph/0606498)
Hadfield L.J., Crowther P.A., Schild H., Schmutz W., 2005, A&A 439, 265
Hamann W-R, Koesterke L, Wessolowski U. 1993 A&A 274, 397
Hanson M.M., Conti P.S., Rieke M.J., 1996, ApJS 107, 281
Herald J.E., Hillier D.J., Schulte-Ladback R.E., 2001, ApJ 548, 932
Hillier D.J., 1985, AJ 90, 1514
Hillier D.J., Jones T.J., Hyland A.R., 1983, ApJ 271, 221
Hillier D.J., Miller D.L., 1998, ApJ 496, 407
Hiltner WA, Schild RE. 1966, ApJ 143, 770
Homeier N., Blum R.D., Conti P.S., Damineli A., 2003a, A&A 397, 585
Homeier N., Blum R.D., Pasquali A., Conti P.S., Damineli A., 2003b, A&A 408, 153
Hopewell E.C., Barlow M.J., Drew J.E. et al. 2005, MNRAS 363, 857
Howarth I.D., Schmutz W., 1992, A&A 261, 503
van der Hucht, K.A., 2006, A&A submitted
van der Hucht, K.A. & Williams, P.M. 2006, A&A in preparation
van der Hucht K.A., Morris P.W. Williams P.M. et al. 1996, A&A 315, L193
Humphreys R.M. 1978 ApJS 38, 309
Indebetouw R., Mathis K.S., Babler B.L., Meade M.R., Watson C. et al. 2005, ApJ 619, 931
Langer N, Hamann W-R, Lennon M, Najarro F, Pauldrach AWA, Puls J. 1994, A&A 290, 819
Leitherer C. et al. 1999, ApJS 123, 3
Levato H., Malaroda, 1980, PASP 92, 323
Marchenko S.V., Moffat A.F.J., Crowther P.A. et al. 2004, MNRAS 353, 153
Martins F, Schaerer D, Hillier DJ. 2005, A&A 436, 1049
Massey P, Thompson A.B., 1991 AJ 101, 1408
Massey P, Johnson J. 1993 AJ 105, 980
Massey, P., Johnson, K.E., DeGioia-Eastwood, K. 1995, ApJ 454, 151
Massey P, DeGioia-Eastwood K, Waterhouse E. 2001, AJ 121, 1050
Mermilliod J.C., 1976, A&A 24, 159
Meynet G., Maeder A., 2003, A&A 404, 975
Meynet G., Maeder A., Schaller G., Schaerer D., Charbonnel C., 1994, A&AS 103, 97
Moffat A.F.J., 1983, A&A 124, 273
Moffat AFJ, Shara MM, Potter M. 1991, AJ 102, 642
Moffat A.F.J., Drissen, L., Shara M.M., 1994, ApJ 436, 183
Morris P.W., Crowther P.A., Houck J.R., 2004, ApJS 154, 413
Muno M.P., Clark J.S., Crowther P.A. et al. 2006, ApJ 636, L41
Negueruela, I., Clark J.S., 2005, A&A 436, 541
Perry C.L., Hill, G., Christodoulou, D.M. 1991, A&AS 90, 195
Rauw G., Crowther P.A., De Becker M., Gosset E., Nazé Y. et al. 2005, A&A 432, 985
Rieke G.H., Lebofsky M.J., 1985, ApJ 288, 618
Rieke G.H., Rieke M.J., Paul A.E., 1989, ApJ 336, 752
Schaerer D., Maeder A. 1992, A&A 263, 129
Schaller G., Schaerer D., Meynet G., Maeder A., 1992, A&AS 96, 269
Schild H., Maeder A., 1984, A&A 136, 237
Skrutskie M.F., Cutri R.M., Stiening R., Weinberg M.D., Schneider S. et al. 2006 AJ 131, 1163
Smith L.F., Shara M.M., Moffat A.F.J., 1996, MNRAS 281, 163
Skinner S.L., Zhekov S.A., Güdel M., Schmutz W., 2002, ApJ 579, 764
Skinner S.L., Simmons A.E., Zhekov S.A., Teodoro M., Damineli A., Palla F, 2006, ApJ 639, L35
Tuthill P.G., Monnier J.D., Danchi W.C., 1999, Nat 398, 487
Vacca W.D., Rayner R.J., Cushing M.C., 2006, ApJ in preparation
Vanbeveren D., De Donter E., Van Bever J. et al. 1998, New Astron 3, 443
Walborn N.R., Howarth I.D., Lennon D.J. et al. 2002, AJ 123, 2754
Westerlund B., 1961, AJ 66, 57
Weidner C., Kroupa P., 2006 MNRAS 365, 1333
Williams P.M., van der Hucht K.A., The P.S., 1987, A&A 182, 91
Williams P.M., 2002, in proc: Interacting Winds from Massive Stars, eds. A.F.J. Moffat & N. St-Louis, ASP: San Francisco, ASP Conf. Ser 260, p.311

APPENDIX A: Absolute magnitudes and intrinsic colours of Wolf-Rayet stars

In this appendix, we provide a calibration of absolute K_S-band magnitudes for (primarily) cluster or association WN and WC stars based upon 2MASS photometry and synthetic J,H,K_S colours. The latter were obtained from convolving CMFGEN (Hillier & Miller 1998) stellar atmosphere models of individual WR stars with SOFI J, H, K_S filter response profiles, with zero points defined by Vega, as is usual. As such, our approach complements the recent empirical JHKL' photometric study for WR stars of van der Hucht & Williams (2006). Dust forming WC stars are excluded from this analysis since their near-IR colours and absolute magnitudes possess a large scatter, with $(J-H)_0 = 1 \pm 0.7$ mag, $(H-K)_0 = 1.1 \pm 0.6$ mag and M_K=–8.5$\pm$ 1.5 mag according to van der Hucht & Williams (2006).

In common with the method outlined within Section 4.1, interstellar K_S-band extinctions are estimated independently using the J–K_S and H–K_S colours of individual cluster/association stars, adopting the Indebetouw et al. (2005) relationship between J, H and K_S extinction. We used the average of the two approaches for our final K_S-band extinction, $\overline{A_{K_S}}$. Absolute magnitudes follow from previously determined cluster/association distance moduli (van der Hucht & Williams 2006).

We have grouped early WN stars according to weak versus strong lined stars, since these stars possess rather different near-IR colours, such that the strong lined stars possess rather stronger stellar winds, and so flatter (free-free) near-IR energy distributions. Our adopted near-IR calibration is presented in Table A1.

Table A1: Calibration of absolute K_S-band magnitudes and intrinsic J,H,K_S colours for Galactic WN3–9 and non-dusty WC5–9 stars, supplemented by two LMC WN10-11 stars, based upon 2MASS photometry and theoretical stellar atmospheric model continua for individual stars. Cluster or association distances are taken from van der Hucht & Williams (2006). A single M_{K_S} is given for WN7–9 stars due to the low number of cluster or association members (WN7ha stars are omitted from the present calibration) whilst M_{K_S} is absent for WC9 stars since neither WR88 nor WR92 are known cluster or association members. Adopted values for each group are shown in bold.

Star	Subtype	$(v\text{-}J)_0$	$(J\text{-}K_S)_0$	$(H\text{-}K_S)_0$	$J\text{–}K_S$	$H\text{–}K_S$	$A_{K_S}^{J-K_S}$	$A_{K_S}^{H-K_S}$	$\overline{A_{K_S}}$	$K_S - \overline{A_{K_S}}$	DM	M_{K_S}
DM	M_K											
		mag	mag	mag	mag	mag	mag	mag	mag	mag	mag	mag
WR46	WN3p	–0.78	–0.11	–0.03	0.37	0.25	0.32	0.51	0.41	9.42	13.05	–3.63
WR152	WN3	–0.78	–0.11	–0.03	0.45	0.28	0.37	0.56	0.47	9.57	12.2	–2.63
WN3–4 (weak)			**–0.11**	**–0.03**								**–3.13**
WR10	WN5h	–0.56	0.04	0.07	0.44	0.28	0.27	0.39	0.33	9.28	13.35	–4.07
WR115	WN6	–0.31	0.17	0.15	1.05	0.48	0.59	0.61	0.60	6.34	11.5	–5.16
WR138	WN5+?	–0.23	0.21	0.17	0.38	0.22	0.11	0.08	0.10	6.38	10.5	–4.02
WR141	WN6+O?	–0.31	0.17	0.15	0.81	0.40	0.43	0.46	0.44	6.09	10.5	–4.41
WN5–6 (weak)			**0.18**	**0.16**								**–4.41**
WR1	WN4b	0.29	0.38	0.27	0.73	0.38	0.23	0.20	0.22	7.26	11.3	–4.04
WR134	WN6b	0.23	0.37	0.27	0.55	0.36	0.12	0.17	0.14	6.02	11.2	–5.18
WR136	WN6b	0.21	0.36	0.26	0.57	0.34	0.14	0.14	0.14	5.42	10.5	–5.08
WN4–7 (strong)			**0.37**	**0.27**								**–4.77**
WR78	WN7h	–0.43	0.09	0.09	0.46	0.29	0.24	0.37	0.31	4.67	11.5	–6.83
WR40	WN8h	0.06	0.28	0.19	0.51	0.30	0.15	0.21	0.18	5.93		
WR66	WN8+?	–0.47	0.07	0.07	0.78	0.33	0.48	0.47	0.47	7.68	12.57	–4.89
WR105	WN9h	–0.56	0.07	0.10	1.30	0.51	0.82	0.75	0.78	4.95	11.0	–6.05
WN7–9 (Weak)			**0.13**	**0.11**								**–5.92**
BE294	WN10h	–0.09	0.29	0.20	0.40	0.29	0.07	0.17	0.12	11.52	18.45	–6.93
S119	WN11h	–0.35	0.07	0.05	0.10	0.13	0.02	0.15	0.08	11.64	18.45	–6.81
WN10–11			**0.18**	**0.12**								**–6.87**
WR111	WC5	0.09	0.66	0.59	0.77	0.63	0.07	0.07	0.07	6.44	11.0	–4.56
WR154	WC6	0.06	0.61	0.59	1.01	0.72	0.26	0.24	0.25	8.04	12.2	–4.16
WR14	WC7	0.09	0.59	0.57	0.88	0.63	0.19	0.10	0.15	6.46	11.5	–5.04
WC5–7			**0.62**	**0.58**								**–4.59**
WR135	WC8	0.07	0.43	0.38	0.57	0.45	0.09	0.12	0.11	6.55	11.2	–4.65
WC8			**0.43**	**0.38**								**–4.65**
WR88	WC9	–0.29	0.23	0.26	0.98	0.51	0.50	0.46	0.48	7.57		
WR92	WC9	–0.29	0.23	0.26	0.68	0.40	0.30	0.26	0.28	8.54		
WC9			**0.23**	**0.26**								

APPENDIX B: Galactic cluster turn-off masses

In Table B1 we list properties for the highest (initial) mass OB stars within Milky Way clusters which contain WR stars. We follow the approach of from Schild & Maeder (1984) and Massey et al. (2001), updated to account for the revised spectral type-$T_{\rm eff}$ calibration of Martins et al. (2005) for O stars, Crowther et al. (2006) for B supergiants, plus the high mass-loss Meynet et al. (1994) Solar metallicity isochrones. A summary of cluster turn-off masses is shown in Table 8.

Table B1: Parameters derived for the highest mass unevolved stars within selected optically visible Milky Way clusters. Parameters for a distance of 2.6 kpc towards the Carina OB1 clusters are listed here, following Humphreys (1978), is preference to the distance of 3.2 kpc derived by Massey & Johnson (1993).

Star	Sp Type	V (mag)	B–V (mag)	E(B–V) (mag)	M_V (mag)	Ref	$T_{\rm eff}$ (kK)	$\log L$ ($L_\odot$)	Mass ($M_\odot$)	Age (Myr)
Cyg OB2 (DM=11.2 mag)										
Cyg OB2 22	O4 III	11.55	2.04	2.36	–7.0	5	42.0	6.22	114	1.8
Cyg OB2 8a	O6 Ib	9.06	1.30	1.60	–7.1	5	37.0	6.13	97	2.0
Cyg OB2 9	O5 If	10.96	1.81	2.11	–6.8	5	38.5	6.05	83	2.0
Cyg OB2 11	O5 If+	10.03	1.49	1.79	–6.7	5	38.5	6.02	80	2.0
NGC 3603 (DM=14.25 mag)										
HD 97950-A2	O3 V	12.0:	1.09:	1.41	–6.6	7	45	6.16	103	1.3
HD 97950-A3	O3 III	12.5:	1.09:	1.41	–6.1	7	44.5	5.95	75	1.1
MDS 42	O3 III	12.8:	1.09:	1.41	–5.8	3	44.5	5.83	64	1.1
MDS 24	O4 V	12.69:	1.09:	1.41	–5.9	3	43	5.83	62	1.6
Pismis 24 (DM=12.0 mag)										
HDE 319718	O3.5 If	10.43	1.45	1.75	–7.0	9,10	41	6.20	108	1.8
Pis 24–17	O3.5 III	11.84	1.49	1.81	–5.8	9,10	43	5.76	57	1.5
Pis 24–2	O5.5 V	11.95	1.41	1.73	–5.4	9	40	5.55	44	2.0
Pis 24–13	O6.5 V	12.73	1.48	1.80	–4.8	9	38	5.26	33	2.0
Trumpler 16 (DM=12.1 mag)										
HD 93250	O3.5 V	7.41	0.17	0.49	–6.2	6,10	45	6.00	80	1.1
HD 93205	O3.5 V	7.76	0.08	0.40	–5.6	6,10	45	5.75	59	1.0
HDE 303308	O4 V	8.19	0.14	0.46	–5.3	6	43	5.60	48	1.3
HD 93204	O5 V	8.48	0.09	0.41	–4.9	6	37	5.53	37	1.3
Havlen–Moffat 1 (DM=12.0 mag)										
LSS 4067	O4 If	11.16	1.54	1.84	–6.5	9	40	6.00	77	1.8
C1715–387 No. 6	O5 If	11.64	1.54	1.84	–6.1	9	38.5	5.76	55	2.3
C1715–387 No. 8	O5 V	12.52	1.52	1.84	–5.2	9	41	5.48	40	1.8
C1715–387 No. 12	O6 If	12.57	1.52	1.82	–5.1	9	39	5.32	33	2.7
NGC 6231 (DM=11.5 mag)										
HD 152234	B0 Iab	5.44	0.20	0.44	–7.4	1,2	27.5	5.90	75:	3.2:
HD 152233	O6 III	6.56	0.14	0.46	–6.4	1,2	38	5.87	63	2.2
HD 152249	O9 Iabp	6.44	0.20	0.48	–6.5	1,2	31	5.70	48	3.2
Collinder 228 (DM=12.1 mag)										
HD 93206	O9.5 I	6.28	0.14	0.41	–7.1	9	30.5	5.90	63	2.7
HD 93632	O5 III	8.39	0.29	0.61	–5.6	9	40.5	5.64	48	2.0
HD 93130	O7 II	8.04	0.27	0.59	–5.9	9	36	5.61	44	2.7
HDE 305525	O6 V	10.00	0.68	1.00	–5.2	9	39	5.43	38	2.2

(1) Mermilliod 1976; (2) Levato & Malaroda 1980; (3) Moffat 1983; (4) Moffat et al. 1991; (5) Massey & Thompson 1991; (6) Massey & Johnson 1993; (7) Moffat et al. 1994; (8) Massey et al. 1995; (9) Massey et al. 2001; (10) Walborn et al. 2002; (11) Corti et al. 2003

Table B1: (continued)

Star	Sp Type	V (mag)	B–V (mag)	E(B–V) (mag)	M_V (mag)	Ref	$T_{\rm eff}$ (kK)	log L ($L_\odot$)	Mass ($M_\odot$)	Age (Myr)
Trumpler 27 (DM=12.0 mag)										
Tr 27–27	O8 III	13.31	2.16	2.47	–6.3	9	34	5.73	51	2.7
LSS 4266	B0.7 Ia	10.11	1.43	1.65	–7.0	9	23	5.59	40	4.2
LSS 4253	B0 Ia	10.55	1.28	1.52	–6.2	9	27.5	5.41	35	4.5
Westerlund 2 (DM=14.5 mag)										
Westerlund 2–18	O7 I	12.81	1.20	1.49	–6.3	4	35	5.75	52	2.7
Westerlund 2–157	O6 V	14.14	1.36	1.68	–5.6	4	39	5.58	44	2.5
Westerlund 2–151	O6 V	14.33	1.33	1.65	–5.3	4	39	5.47	39	2.5
Westerlund 2–167	O7 V	14.19	1.29	1.61	–5.3	4	37	5.41	36	2.7
Berkeley 87 (DM=11.0 mag)										
HDE 229059	B1 Ia	8.71	1.52	1.71	–7.6	9	21.5	5.76	49	3.7:
Berk 87–25	O8.5 III	10.46	1.29	1.60	–5.5	9	33	5.35	32	4.0
Berk 87–4	B0.2 III	10.92	1.26	1.53	–4.8	9	28.5	4.98	21	2.0
Pismis 20 (DM=12.7 mag)										
HD 134959	B2.5 Ia	8.20	0.93	1.08	–7.8	9	16.5	5.63	39	4.5
Pis 20–2	O8.5 I	10.45	0.71	1.00	–5.4	9	32	5.26	29	4.5
NGC 6871 (DM=11.65 mag)										
HD 226868	O9.7 I	8.81	0.83	1.09	–6.2	8	30	5.60	38	3.9
HD 190864	O7 III	7.77:	0.18:	0.50	–5.4	8	36	5.43	36	3.2
HD 227018	O7 V	8.96	0.37	0.69	–4.8	8	37	5.22	31	2.5
Berkeley 86 (DM=11.4 mag)										
HDE 228841	O7 V	8.98	0.60	0.92	–5.3	8	37	5.40	37	2.7
HD 228943	B0 V:	9.30	0.87	1.17	–5.7	8	29.5	5.31	30	4.7:
HD 193595	O8 V	8.70	0.37	0.68	–4.8	8	28	5.15	28	3.5
HDE 228969	O9.5 V	9.49	0.68	0.98	–4.9	8	32	5.10	25	5.0:
Bochum 7 (DM=13.45 mag)										
LSS 1131	O7.5 V	10.80	0.51	0.82	–5.2	11	36.0	5.33	33	3.2
LSS 1135	O6.5 V	10.88	0.40	0.72	–4.8	11	38.0	5.24	32	2.2
LSS 1144	O7.5 V	11.27	0.64	0.95	–5.1	11	36.0	5.31	32	3.2
Ruprecht 44 (DM=13.35 mag)										
LSS 891	O8 III	10.93	0.29	0.60	–4.3	9	34	4.90	22	3.5
LSS 920	O9.5 V	11.38	0.24	0.54	–3.6	9	31.5	4.56	17	3.5
Markarian 50 (DM=12.8 mag)										
HD 219460A	B0 III	10.7:	0.52	0.79	–4.5	9	28.5	4.80	18	7.0:
Ma 50–31	B0.5 II	11.21	0.64	0.86	–4.3	9	26.0	4.60	15	10.:

(1) Mermilliod 1976; (2) Levato & Malaroda 1980; (3) Moffat 1983; (4) Moffat et al. 1991; (5) Massey & Thompson 1991; (6) Massey & Johnson 1993; (7) Moffat et al. 1994; (8) Massey et al. 1995; (9) Massey et al. 2001; (10) Walborn et al. 2002; (11) Corti et al. 2003